INORGANIC CHEMISTRY FRONTIERS

RESEARCH ARTICLE

View Article Online
View Journal | View Issue

Cite this: *Inorg. Chem. Front.*, 2026, **13**, 1013

Chemical characterization of localized radicals in *closo*-borate anion derivatives

Jaskiran Kaur, †[a] Markus Rohdenburg, †[b] Kirsten Zeitler, [c] Judy K. Y. Liu,[a] Carsten Jenne, [d] Maik Finze, [e] Hilkka I. Kenttämaa [a] and Jonas Warneke *[b,f]

The conceptual understanding of the reactivity of localized main group element radicals in molecules and ions has so far been strongly focused on carbon radicals in organic compounds. In this study, permanent anions with a radical site localized on the vacant vertex of icosahedral *closo*-dodecaborate anions and 1-carba-*closo*-dodecaborate anions have been characterized by both various (radical) ion-molecule reactions in the gas phase and by computational investigations, including conceptual DFT, potential energy surfaces (PES) and energy decomposition analysis (EDA). The reactivity of these radical ions towards electron-deficient and electron-rich double bonds as well as their halogen and hydrogen atom abstraction reactions have been studied. The radical ions were varied with respect to their charge state, the nature of the spin-carrying atom and their substituents. Additionally, their reactivity was compared with that of prototypical electrophilic and nucleophilic aryl radicals. Interestingly, not all the (di)anionic radicals are nucleophilic; particularly the ion $[CB_{11}I_{11}]^{\bullet-}$ was characterized as highly electrophilic. Furthermore, simple categorization based on "polarity matching" arguments is not sufficient to fully explain the reactivity of these radical ions towards allyl iodide. Element-specific spatial extension of the spin density and non-covalent interactions of the allyl iodide with the *closo*-borate or *closo*-carborate anion framework determine the transition state geometries and energies and therefore strongly influence the relative rate of competing reactions. These results showcase both the transferability and the limitations of "classical" concepts (as typically applied successfully in organic chemistry) for the characterization of ionic borane cluster radicals. Our approach represents a broadly applicable, general method for understanding radical reactivity towards a broad range of reaction partners.

Received 23rd October 2025,
Accepted 21st November 2025

DOI: 10.1039/d5qi02163d

rsc.li/frontiers-inorganic

1. Introduction

Understanding the chemical nature of localized radicals is essential for controlling the selectivity of these highly reactive species in chemical reactions. Although conceptual approaches to categorize radical reactivity have comprehensively been explored for organic radicals (*e.g.*, polarity match),[1–3] knowledge on transferability and generalization of these concepts remains largely lacking. Especially localized radicals within small multiply charged anions (MCAs) have rarely been studied experimentally. In the condensed phase, localized radicals tend to react very fast, making their characterization challenging and usually only possible with ultrafast spectroscopy applied during radical formation.[4–7] Investigating reactions of a selected ionic radical with defined reagents is possible in mass spectrometers because highly reactive radicals exhibit extended lifetimes in the low-pressure regimes and can collide with gaseous reagents leaked into a vacuum chamber.[8] However, such studies are often not applicable to multiply charged anionic radicals, as they tend to autodetach electrons in the gas phase, thereby limiting their lifetimes.[9,10] Electron loss is often facilitated by both intramolecular Coulomb repulsion and the formation of an even-electron ion. One strategy to observe doubly charged molecular radical anions in the gas phase is the spatial separation of the charge from the localized radical center in extended molecular structures, which is realized in so-called distonic radical ions. In such cases, the influence of the charge on the reactivity of the

[a]*James Tarpo Jr and Margaret Tarpo Department of Chemistry, Purdue University, 560 Oval Drive, West Lafayette, IN, 47907, USA*
[b]*Wilhelm-Ostwald-Institut für Physikalische und Theoretische Chemie, Universität Leipzig, Linnéstr. 2, 04103 Leipzig, Germany. E-mail: jonas.warneke@uni-leipzig.de*
[c]*Institut für Organische Chemie, Universität Leipzig, Johannisallee 29, D-04103 Leipzig, Germany*
[d]*Anorganische Chemie, Fakultät für Mathematik und Naturwissenschaften, Bergische Universität Wuppertal, Gaußstr. 20, 42119 Wuppertal, Germany*
[e]*Institut für Anorganische Chemie, Institut für Nachhaltige Chemie & Katalyse mit Bor (ICB), Julius-Maximilians-Universität Würzburg, Am Hubland, 97074 Würzburg, Germany*
[f]*Leibniz Institute of Surface Engineering (IOM), Permoserstr. 15, 04318 Leipzig, Germany*
†These authors contributed equally.

radical site can be small if the charge and radical sites are widely separated in space.[11] The formation of multiply charged radical anions, which exhibit a localized radical site in close proximity strongly influenced by the negative charge, may only be possible through homolytic bond cleavage within MCAs that possess exceptionally high electronic stability.

The *closo*-dodecaborate dianions $[B_{12}H_{12}]^{2-}$ and their derivatives are well known boron compounds of interest to various applications in medicine and materials science.[12–21] The halogenated derivatives $[B_{12}X_{12}]^{2-}$ (X = halogen), and, in particular, the percyanated derivative $[B_{12}(CN)_{12}]^{2-}$, exhibit exceptional electronic and structural stability.[22,23] These dianions and their singly charged 1-carba-*closo*-dodecaborate anion analogues $[HCB_{11}X_{11}]^{-}$ (abbr. as *closo*-carborate anion) have been used to stabilize highly reactive cations in chemical synthesis and catalysis.[24] However, reports on selective homolytic cleavage of stable B–X bonds (with X = halogen) remain scarce. Yet, some photochemical approaches have been recently published that demonstrate the substitution of X in solution, but potential intermediates and reaction mechanisms remain speculative.[25] The heterolytic cleavage of a B–X bond in *closo*-$[B_{12}X_{12}]^{2-}$ ions has been extensively studied in the gas phase by using collision-induced dissociation (CID) of either $[B_{12}X_{12}]^{2-}$ or ion pairs $[B_{12}X_{12}]^{2-}[M]^{+}$ yielding the fragment ion $[B_{12}X_{11}]^{-}$ (for X = F, Cl, Br, I, CN, pathway **1**, see Fig. 1). The $[B_{12}X_{11}]^{-}$ ion is among the most reactive even-electron anions known today, as evidenced by its spontaneous binding to noble gases and alkanes.[23,25–28] Despite its negative charge, $[B_{12}X_{11}]^{-}$ is highly electrophilic due to a positive partial charge on the vacant boron atom. Another possible reaction of $[B_{12}X_{12}]^{2-}$ is electron detachment yielding $[B_{12}X_{12}]^{\bullet-}$ ions (pathway 2, see Fig. 1). The unpaired electron is delocalized, thus rendering these radical anions rather unreactive. $[B_{12}X_{12}]^{\bullet-}$ radical ions have been studied in both gas and condensed phase.[29] In contrast, homolytic cleavage of a B–X bond yields the radical dianion $[B_{12}X_{11}]^{\bullet2-}$ with the radical site strongly localized at the vacant boron atom (pathway 3, see Fig. 1). The radical reactivity of these anions manifests itself, for example, in reactions with (triplet) oxygen $^3O_2$, which have been investigated for $[B_{12}I_{11}]^{\bullet2-}$ and $[HCB_{11}I_{10}]^{\bullet-}$ in a previous study.[30] Apart from these experiments with oxygen, no further characterization or experimental investigation of the reactivity of these (di)anionic radicals have been performed. Recent computational studies demonstrated the high electronic stability of the dianionic radicals $[B_{12}X_{11}]^{\bullet2-}$ and proposed that the binding of $[B_{12}X_{11}]^{\bullet2-}$ to N_2 and CO_2 leads to a considerable activation of these stable molecules.[31] However, binding of N_2 has experimentally only been observed for the even-electron $[B_{12}X_{11}]^{-}$ ions (pathway 1) at room temperature and was never observed for $[B_{12}I_{11}]^{\bullet2-}$ in experimental studies at room temperature. Therefore, such computationally predicted activation is likely only relevant for gas-phase reactions at cryogenic temperatures, which allows the study of weakly bound complexes.

The aim of the present study is to characterize the reactivity of localized radicals at the "vertex of anionic borane ico-

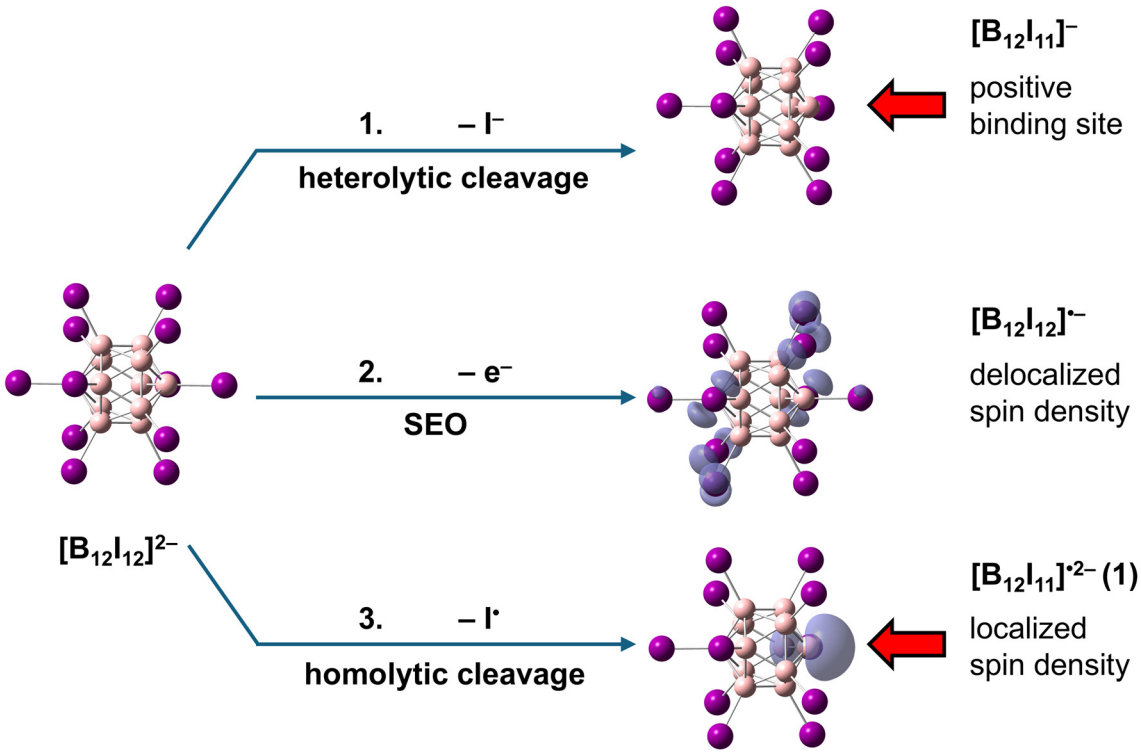

Fig. 1 Three possible fragmentation pathways of $[B_{12}I_{12}]^{2-}$. Pathways 1 and 3 are observed during CID of $[B_{12}I_{12}]^{2-}$. Pathway 2 requires the presence of a strong oxidizing agent. Semi-transparent spin density isosurface representations derived from DFT calculations are shown in pathway 2 and 3 (isosurface representations are displayed at an isovalue of 0.003). SEO = single electron oxidation.

sahedra" – an exceptional radical site that can exist within isolated dianions. The chemical character of a radical is often conceptually described by features such as nucleophilic/electrophilic properties and polarity matching between the radical and the substrate. Although these intuitive (kinetic) concepts are well established for organic radicals and are successful in describing differences in radical reactivity (*e.g.*, alternating co-polymerization),[32] they are difficult to transfer to the less intuitively accessible *closo*-borate anion radicals. Here, we investigate the reactivity of several *closo*-borate and *closo*-carborate radical anions that we selectively generated in the gas phase ($[B_{12}I_{11}]^{\bullet 2-}$ (**1**), $[B_{12}(CN)_{11}]^{\bullet 2-}$ (**2**), $[HCB_{11}I_{10}]^{\bullet -}$ (**3**), $[CB_{11}I_{11}]^{\bullet -}$ (**4**), and $[B_{12}Br_{11}O]^{\bullet 2-}$ (**5**)) towards neutral reagents introduced into an ion trap (dimethyl disulfide, styrene, methyl acrylate, carbon tetrachloride, allyl iodide and allyl chloride). The results provide insights into the role of different ionic parameters on the reactivity of the radical, *e.g.*, the ion charge, the boron-bound substituents and the nature of the atom on which the spin density is localized.

Striking differences in the reactivity of *B*- vs. *C*-connected carboranyl derivatives, such as in phosphine ligands, characterize the boron vertex as electron rich and the carbon vertex as electron poor.[33] However, detailed studies on the "philicity" of *B*- or *C*-centered radicals in borate and carborate cluster derivatives remain elusive.

Due to their delocalized σ-electron system, *closo*-borate anions exhibit three-dimensional aromaticity.[34] Therefore, we compare the reactivity of *closo*-borate and -carborate radical anions with the reactivity of organic aromatic radical ions such as distonic quinoline-based radical cations[35,36] and phenyl derivatives covalently coupled to a charge-tag (*e.g.*, $-BF_3^-$).[11,37] Computational chemistry is used to understand the differences in the reaction behavior of the radicals by computing potential energy surfaces (PES) for the reactions and applying "conceptual DFT" (cDFT).[2,3,38] This allows us to assign a "chemical character" to localized radicals in *closo*-dodecaborate anions and their derivatives.

The increased use of boranes and carboranes as bioisosteric arene mimetics, for instance in the functionalization of biomolecules or within organocatalytic frameworks, has given rise to novel radical-based synthetic methodologies.[39–43] A more detailed and conceptual understanding of these intermediate radicals and their reactivity could further facilitate the elucidation of mechanisms involved in the increasingly important photochemical synthesis of dodecaborate derivatives[23,44] as well as radical[45,46] and photocatalytic[47] approaches to functionalize, for example, biomolecules with boranes or carborane moieties.

In addition, the investigation of the reactivity of gaseous dodecaborate anion radicals is an important preliminary work for applying these ions in preparative mass spectrometry experiments, as for example, enabling the controlled synthesis of new compounds in surface layers by using reactive gas-phase ions or the selective, covalent charge-tagging of biomolecules at interfaces.[28,48–50]

2. Methods

2.1 Mass spectrometry

All mass spectrometry experiments were conducted using a modified Thermo Scientific LTQ linear quadrupole ion trap (LQIT) mass spectrometer equipped with an electrospray ionization (ESI) source. The analyte solutions were prepared in methanol and were directly introduced into the ESI source at a flow rate of 10–15 μL min^{-1} by using a 500 μL Hamilton syringe. The ESI source conditions used were 3 kV spray voltage, 20–30 (vendor-specific arbitrary units) of sheath gas (N_2), 10 (vendor-specific arbitrary units) of auxiliary gas (N_2), and 275 °C capillary temperature. After ionization of the analytes, the ions were transferred into the ion trap, isolated using an isolation width of 0.5–2.0 *m*/*z*-units and a *q* value of 0.25 and were allowed to react with different reagents for up to 10 000 ms before all ions were ejected for detection. Reagents were introduced into the ion trap (containing 2 mTorr of helium buffer gas) *via* an external reagent mixing manifold similar to that first proposed by Gronert.[51] The reagents were introduced into the manifold by using a syringe pump at a flow rate of 2–5 μL h^{-1} and diluted with helium before entering the ion trap through a variable leak valve. For collision-induced dissociation experiments (CID), the advanced scan features of the LTQ Tune Plus interface were used. The isolated ions were subjected to CID (collision energy 20–55 arbitrary units) for 30 ms by using helium as the collision gas. All mass spectra acquired were an average of at least 15 individual mass spectra. Xcalibur 2.0 software was used to process the data.

Note: *closo*-Borate anion derivatives show broad isotopic patterns in mass spectra due to the multiple possible combinations of the abundant ^{11}B and ^{10}B isotopes. Here, the above-mentioned narrow isolation width targets the isolation of all ions with one nominal *m*/*z* value. This results in a clearer determination of *m*/*z* differences in the spectrum, *e.g.*, upon adduct formation or H atom addition. However, due to technical reasons, ions with one *m*/*z* unit higher or lower can often not be fully excluded during the isolation process. In such cases, the same pattern of the reagent ion observed in mass spectra is observed for the product ion (if the isotopic pattern of the added molecule/atom is negligible).

2.2 Computational studies

DFT calculations were performed using the Gaussian 16, rev. C.02 program.[52] Geometry optimization was carried out on B3LYP-D3(BJ)/def2-TZVPP level.[53–58] Subsequent frequency calculations were performed to ensure that the obtained stationary points are either minima or transition states on the potential energy surface (PES). In addition, the PES was evaluated for selected examples on M06-2X[59]-D3[57]/def2-TZVPP level. This method has previously been applied successfully to find optimized geometries for the collision complex (CC) and the transition state (TS).[60–62] For 0 K attachment enthalpies ($\Delta H_{0\ K}$), the Basis Set Superposition Error (BSSE) was corrected for in a counterpoise[63,64] calculation on the optimized adduct geometry. All outputs of relevant calculations are published in

ioChem-BD and can be retrieved under the following link: https://doi.org/10.19061/iochem-bd-6-587.

Conceptual DFT (cDFT) calculations were performed with the Multiwfn program, version 3.8.[65,66] The cDFT implementation used in Multiwfn was described previously.[67] To perform cDFT analysis, the optimized geometries and their respective wavefunction files were taken from Gaussian 16 runs. Additional wavefunction files for N, $N+1$, $N-1$, and $N-2$ electronic states were computed as single point calculations with the ORCA program, version 6.0[68,69] using a B3LYP/G-D3(BJ)/def2-TZVPP level.

Energy decomposition analysis (EDA) was performed within the sobEDA framework[70] by partitioning the total interaction energy (ΔE_{int}) between two fragments into components due to electrostatic interaction (ΔE_{els}), exchange interaction (ΔE_x), repulsion interaction (ΔE_{rep}), orbital interaction (ΔE_{orb}), DFT correlation (ΔE_{DFTc}) and dispersion correction (ΔE_{dc}). ΔE_x and ΔE_{rep} are typically merged to give an exchange-repulsion term ΔE_{xrep} ($\Delta E_{xrep} = \Delta E_x + \Delta E_{rep}$) in the suggested sobEDA scheme. We further combine the exchange-repulsion term with the DFT correlation to yield a condensed Pauli repulsion-type interaction component ($\Delta E_{Pauli} = \Delta E_{xrep} + \Delta E_{DFTc}$). This term is intended to resemble the Pauli repulsion in the Morokuma-Ziegler EDA partitioning scheme.[71–73]

2.3. Synthesis of precursor salts

Salts of the anions $[1\text{-}HCB_{11}I_{11}]^-$,[74] $[B_{12}I_{12}]^{2-}$,[75,76] $[B_{12}(CN)_{12}]^{2-}$,[23] and $[B_{12}Br_{11}NO_2]^{2-}$,[77] were synthesized according to previously established procedures. $[1\text{-}IHg\text{-}CB_{11}I_{11}]^-$ was generated *via* CID in an ion trap from a reaction mixture initially obtained from HgI_2, *n*BuLi, and Cs[1-$HCB_{11}I_{11}$], which also contained a minor amount of $[1\text{-}HCB_{11}I_{10}\text{-}12\text{-}C_4H_9]^-$.[78]

3. Results and discussion

3.1 Generation of localized radical sites in *closo*-dodecaborate and carborate anions

$[B_{12}I_{11}]^{\bullet 2-}$ (1). CID of $[B_{12}I_{12}]^{2-}$ generates the radical dianion **1** by the elimination of $I^\bullet$ (eqn (1)). The spin density is localized on the vacant boron atom as shown in Fig. 2. This reaction competes with the elimination of an iodide (I^-) to generate $[B_{12}X_{11}]^-$.

$$[B_{12}I_{12}]^{2-} \xrightarrow[-I^\bullet]{CID} [B_{12}I_{11}]^{\bullet 2-} \quad (1)$$

$[B_{12}(CN)_{11}]^{\bullet 2-}$ (2). CID of $[B_{12}(CN)_{11}I]^{2-}$ generates the cyano derivative **2** by the elimination of $I^\bullet$ (eqn (2)). The spin density is localized on the vacant boron atom as shown in Fig. 2. It should be noted that $[B_{12}(CN)_{12}]^{2-}$ is a highly stable ion and thus does not serve as a suitable precursor for ion **2**.[23]

$$[B_{12}(CN)_{11}I]^{2-} \xrightarrow[-I^\bullet]{CID} [B_{12}(CN)_{11}]^{\bullet 2-} \quad (2)$$

$[HCB_{11}I_{10}]^{\bullet -}$ (3). CID of $[HCB_{11}I_{11}]^-$ results in the formation of a radical anion with molecular formula $[HCB_{11}I_{10}]^{\bullet -}$ (**3**) by homolytic cleavage of $I^\bullet$ (eqn (3)). A mixture of three different isomers is expected to form (with the vacant boron site being located *ortho*, *meta* or *para* with respect to the CH group). We target to generate the isomer with the vacant boron atom in the *para* position to the CH group so that the steric and electronic situation for the generated radical site is similar to that of the radical site in $[B_{12}I_{11}]^{\bullet 2-}$ (the spin density-carrying vacant boron atom is surrounded by five iodine substituents). Therefore, the precursor $[1\text{-}HCB_{11}I_{10}\text{-}12\text{-}C_4H_9]^-$ was used for this study. CID induces a homolytic B–C bond cleavage in this precursor to generate the *para*-$[HCB_{11}I_{10}]^{\bullet -}$ (**3**), see Fig. 2.

$$[1\text{-}HCB_{11}I_{10}\text{-}12\text{-}C_4H_9]^- \xrightarrow[-C_4H_9^\bullet]{CID} [1\text{-}HCB_{11}I_{10}]^{\bullet -} \quad (3)$$

$[CB_{11}I_{11}]^{\bullet -}$ (4). CID of $[IHg\text{-}CB_{11}I_{11}]^-$ leads to the homolytic cleavage of the Hg–C bond and results in the formation of **4** (eqn (4)). The spin density is localized on the carbon atom as shown in Fig. 2.

$$[IHg\text{-}CB_{11}I_{11}]^- \xrightarrow[-HgI^\bullet]{CID} [CB_{11}I_{11}]^{\bullet -} \quad (4)$$

$[B_{12}Br_{11}O]^{\bullet 2-}$ (5). CID of $[B_{12}Br_{11}NO_2]^{2-}$ results in the elimination of the stable NO radical and formation of a B–O bond (eqn (5)).[77] The spin density is localized on the oxygen atom and exhibits a p-orbital shape, as shown in Fig. 2, and hence clearly differs from the radical anions **1–4** where the radical site is localized at the vacant boron/carbon atom of the cage.

$$[B_{12}Br_{11}NO_2]^{2-} \xrightarrow[-NO^\bullet]{CID} [B_{12}Br_{11}O]^{\bullet 2-} \quad (5)$$

In several of the following investigations, the reactivities of the radical ions **1–5** are compared with the corresponding reactivity of organic distonic radicals of both polarities.

$[C_9H_7N]^{\bullet +}$ (Q). Protonated 6-iodoquinoline was used as a precursor. CID results in the elimination of $I^\bullet$ (eqn (6)). The spin density is localized on the vacant carbon atom, as shown in Fig. 2.

$$[C_9H_7IN]^+ \xrightarrow[-I^\bullet]{CID} [C_9H_7N]^{\bullet +} \quad (6)$$

$[C_6H_4BF_3]^{\bullet -}$ (B). 3-Iodophenyltrifluoroborate anion was used as a precursor for the generation of this organic radical anion. The elimination of $I^\bullet$ yielding **B** is only a side reaction pathway (eqn (7)). Predominantly, I^- elimination was observed.

$$[C_6H_4BF_3I]^- \xrightarrow[-I^\bullet]{CID} [C_6H_4BF_3]^{\bullet -} \quad (7)$$

3.2. Reactions with dimethyl disulfide (DMDS)

The thiomethyl abstraction reaction from dimethyl disulfide (DMDS) has been established in previous studies to confirm the chemical availability of localized radical sites in gaseous ions.[79] All the ions shown in Fig. 2 indeed exhibit this reactivity, demonstrating the presence of a reactive radical site within all the ions. A product at +47 u (thiomethyl addition) was observed in all cases when DMDS was introduced as neutral reagent gas into the ion trap (see mass spectra in Fig. S1). The oxygen-centered radical of ion **5** showed a competing reaction by abstracting $H^\bullet$ from DMDS.

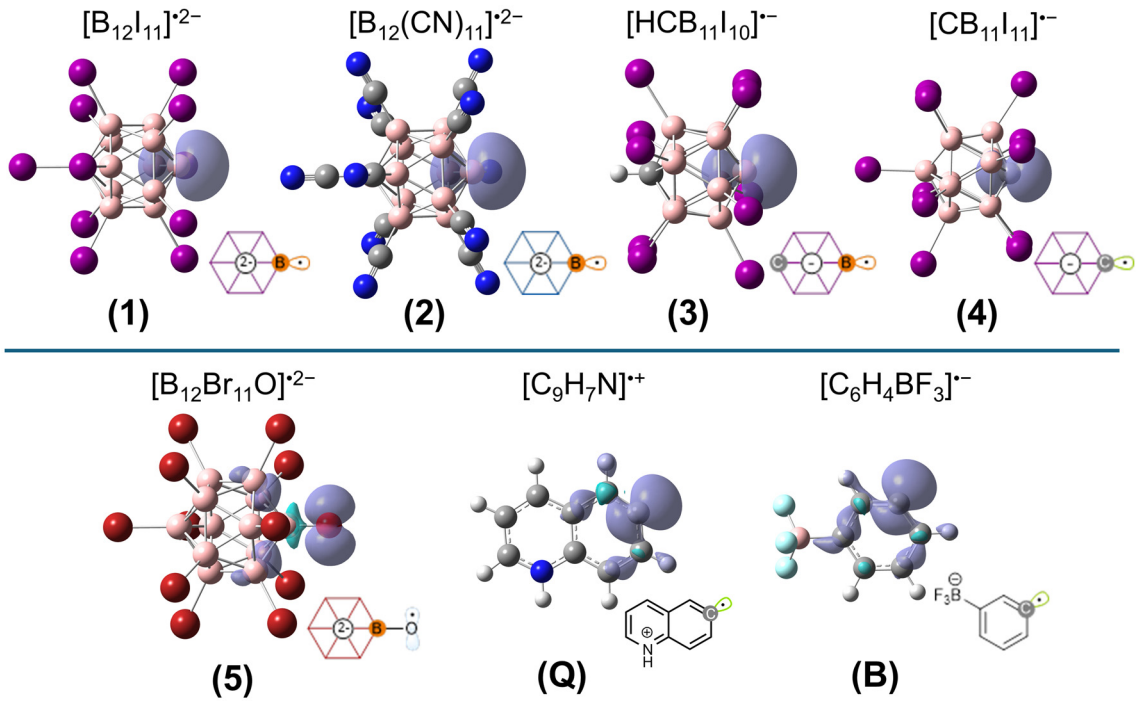

Fig. 2 DFT-calculated optimized geometries and semi-transparent isosurface representations of the spin density (α−β spin) of the five *closo*-borate radical anion derivatives **1–5** and the two organic radical ions **Q** and **B** investigated in this study. Isosurface representations are displayed at an isovalue of 0.003. At the bottom right of each geometry, a pictogram is introduced, which will be used throughout the results section to signify the respective radical ions.

3.3. Reactivity with methyl acrylate and styrene

A mixture of methyl acrylate (**MA**) and styrene (**ST**) (see structures in Fig. 3a) was introduced into the ion trap for reactions with the borane radical ions **1–5** and the organic ions **Q** and **B**. **MA** has an electron-deficient C=C bond while **ST** exhibits a more electron-rich C=C bond. These two reagents were chosen because both of them form stable adducts with radical ions **1–5**, **Q** and **B** with similar reaction enthalpies (see Table 1 and mass spectra in Fig. S2 and S3). Therefore, the different abundance ratios of **MA** and **ST** products might directly correlate with their respective affinities for electron-poor or electron-rich double bonds. The formed adducts are likely efficiently thermalized by collisions in the ion trap.[80] It should be noted that the exact ratio of the two reagents in the ion trap cannot be controlled by us with the available experimental setup. Therefore, the observed abundance ratio of **MA** and **ST** products for a given ion do not necessarily reflect its affinity because the ratio of **MA** and **ST** in the gas phase during the reaction is unknown. However, this ratio of the two components was kept constant over the duration of the experiments with all ionic radicals. Therefore, the changes in the abundance ratio of **MA** and **ST** products within the series of probed radical ions may provide insights into their different binding affinities.

Fig. 3a shows the mass spectra obtained for reactions of ions **1–5** with the gas mixture of **ST** and **MA**. In addition to the signals of the stable adducts with **MA** and **ST**, less abundant products formed upon O_2 binding were also observed (see Fig. S4 for the full mass spectrum). For the organic cationic radical **Q**, the **ST** adduct marked in orange was observed in higher abundance than the **MA** adduct marked in green in Fig. 3. The reaction is much slower for ion **B** and instead, other product ions are observed, which are known decomposition products of ion **B** after binding O_2.[11] For anion **B**, only the **MA** adduct and no **ST** adduct was observed (see Fig. S5 for zoomed-in mass spectrum). For dianions **1** and **2**, the **MA** adducts are >200% more abundant than the **ST** adducts. Therefore, the reaction behavior of these dianions shows more similarities with the reaction behavior of anion **B** than with cation **Q**. For the singly charged ion **3**, the relative abundance of the **ST** adduct is greater than for **1** and **2**. In contrast to the borane radicals with vacant boron center, the **ST** adduct is more abundant for ions **4** and **5** than the MA adduct. Therefore, the reaction behavior of these two anions is more similar to the reaction behavior of the cation **Q** than to the reaction behavior of anion **B**.

Dianions **1** and **2** show similar reactivity and binding enthalpies, despite their different substituents. Although the reactivity of the even electron ions $[B_{12}X_{11}]^-$ has been shown to depend on the substituents X,[81] this does not appear to be the case for $[B_{12}X_{11}]^{\bullet 2-}$. The strongly preferred binding of electron deficient **MA** by ions **1** and **2** and an increased affinity of ion **3** towards the more electron-rich **ST** indicates that **1** and **2** are more nucleophilic/less electrophilic than the singly charged analogue **3**. Reduced nucleophilicity/increased electrophilicity

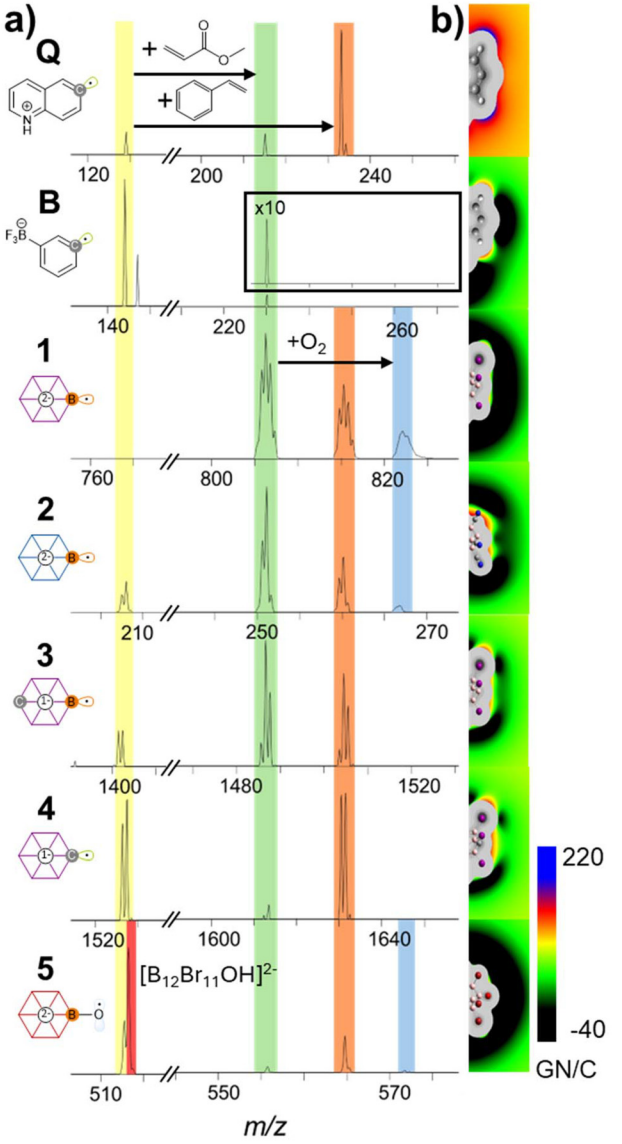

Fig. 3 (a) Mass spectra obtained after 1000 ms reaction between isolated ions **1**–**4**, **B**, and **Q** with a mixture of **MA** and **ST** and 3000 ms reaction time between isolated ion **5** with a mixture of **MA** and **ST** in the ion trap of a linear quadrupole ion trap mass spectrometer. The isolated radical ion is marked in yellow. The products formed after binding with **MA** and **ST** are marked green and orange, respectively. The ion formed by O_2 binding of the **MA** adduct is marked in blue. In the case of ion **5**, H atom abstraction occurs as the major reaction pathway and the product is marked in red, for details see Fig. S6. (b) Electric field in front of the vacant sites of ions **1**–**5**, **B**, and **Q**. Green to black areas mark regions of increasing repulsive field strength on a negative point charge while red to blue areas indicate attraction on a negative point charge. The electron density regions within the molecular surface (0.001 a.u. isosurface) have been colored grey. The electric field strength was computed by numerically differentiating the electrostatic potential with respect to the atomic coordinates of the vacant sites of the respective ions. GN/C = GigaNewton per Coulomb.

is intuitively expected for a lower negative charge state. Remarkably, the carborate anion radical **4** shows a product ratio similar to that of the organic cation **Q**, indicating that this borate anion with the localized spin density on a vacant carbon atom should be described as strongly electrophilic similar to a phenyl cation. A similar ratio of **MA** and **ST** products, as observed for ion **4**, was observed for the dianion **5** with a localized oxygen radical site, but H atom abstraction is the dominant reaction channel. The typical H atom acceptor property of oxygen-localized radicals known from organic oxygen radicals[56] is apparently not significantly affected by the double negative charge of the ion, although it has been reported that negative electric fields or the presence of negative charge-tags increase the barrier for H atom abstraction as compared to neutral radicals.[82]

3.4. Conceptual descriptors of electrophilic and nucleophilic reactivity

Partial positive/negative charge at the reactive site of an ion is an indicator of its electrophilic/nucleophilic reactivity. We computed the electric field surrounding all the investigated ions by calculating the first derivative of the electrostatic potential (ESP) with respect to the nuclear coordinates of the vacant atoms for all investigated ions. A two-dimensional visualization is provided in Fig. 3b. The ESP plotted on the molecular surface of the probed ions can be found in Fig. S7. As can be expected from the overall charge state of the ions, only cation **Q** exhibits a long-range attraction for negative charges as shown by orange and red color, while the anions exhibit long-range repulsive forces as shown by green to black colors. However, there is a distinct difference in the magnitude of the field strength in close vicinity to the vacant sites: ions **1**, **2** and **5** exhibit a highly repulsive region for negative charge with field strengths exceeding 40 GN/C directly in front of the vacant site while carborates **3** and especially **4** show a reduced repulsive field. In the case of **4**, the area close to the vacant carbon atom may be described as an "entrance channel" that could allow for nucleophilic reagents to approach the ion without substantial repulsion (light green path). Remarkably, close to the molecular surface, anion **4** possesses attractive force on negative charges. We conclude that the electric field near the radical site promotes a strong nucleophilic reactivity for radical anions **1**, **2**, and **B**, a weaker nucleophilic reactivity for ion **3** and an electrophilic reactivity for ions **4** and **Q**. This is in line with the experimentally observed reactivity shown in Fig. 3a towards the competition experiments with the mixture of **MA** and **ST**. On the other hand, the strong electrophilic reactivity of ion **5** cannot be promoted by the electric field near the binding site, since a repulsive force is expected for nucleophiles.

To gain further independent insight, we used conceptual DFT (cDFT) that allows us to assign global electrophilicity (ω) and nucleophilicity (ω^-) indices to chemical species, which can be further condensed to their atoms yielding local indices ω^X (here: X = C, B or O) and can be used to characterize the vacant atoms of the investigated radicals. Table 1 lists the calculated values. We encountered methodological problems during assigning ω and ω^- to charged species by using cDFT.

Table 1 0 K attachment enthalpies (B3LYP-D3(BJ)/def2-TZVPP) for the reactions of radical ions **1**–**5**, **Q** and **B** with **MA** and **ST** and global and local cDFT descriptors for their artificially neutralized forms. Note that **5** as an O-centered radical has a strong preference for H atom abstraction in comparison to adduct formation and is thus highlighted in grey. Also note that the attachment enthalpies slightly deviate from the values plotted in the diagram in Fig. 3 due to differences in the computational method. ω = electrophilicity index, ω^- = nucleophilicity index, $\omega^X/\omega^{-,X}$ = local electrophilicity/nucleophilicity index for atom X. Red and blue font color mark the two highest local electrophilicity and nucleophilicity values (highest: bold), respectively

Ion	Enthalpy **MA** binding (kJ mol^{-1})	Enthalpy **ST** binding (kJ mol^{-1})	Neutralized form	Global ω (eV)	Local ω^X (e·eV)	Global ω^- (eV)	Local $\omega^{-,X}$ (e·eV)
1	−199	−208	**1**-Mg	2.47	0.16	3.32	**0.74**
2	−203	−209	**2**-Mg	3.30	0.46	1.56	0.48
3	−190	−199	**3**-Na	2.53	0.30	3.01	0.65
4	−166	−180	**4**-Na	4.28	**0.78**	2.71	−0.14
5	−107	−126	**5**-Mg	3.23	0.95	2.04	0.01
Q	−185	−218	**Q**-F	1.69	**0.61**	1.96	0.54
B	−174	−181	**B**-Na	1.20	0.26	3.16	**0.87**

The calculation of the electrophilicity index ω uses ionization potentials (IP) and electron affinities (EA), which describe the energy required to bring an electron from the radical to infinite distance, or the energy gained by the approach of an electron from infinite distance and its attachment to the radical, respectively. Describing electrophilicity based on these two physical quantities is thus based on the assumption that the energetics of receiving electron density from a reagent correlates with the energetics of attaching an electron approaching from infinity. Similarly, it is assumed that the energetics of providing electron density from a radical to a reactant correlates with IP. These assumptions conceptually appear reasonable for neutral radicals and have successfully predicted trends in radical selectivity towards electrophilic and nucleophilic reaction partners.[1,2] However, we want to raise attention about issues with a direct transfer of this concept to *ionic* radicals: if a radical carries a non-zero charge, the energetics of electron attachment (value of EA) and electron detachment (value of IP) are largely determined by the long-range Coulomb interaction between two charges (ion & electron), whereas receiving or releasing of electron density for bond formation with a neutral reaction partner is not. A more detailed explanation of the problem is given in section S8 of the SI. To circumvent this problem and to be able to assign chemically meaningful values for the local cDFT descriptors, we artificially included counterions (Na^+ for anions, Mg^{2+} for dianions and F^- for cation **Q**) into the computational investigation of the ionic radicals and located them spatially separated from the radical site of the ion to ensure the least possible disturbance of the radical site. The organic radical anion **B**, as well as the borate (di)anions **1**–**3**, show a higher local nucleophilicity index than electrophilicity index on their vacant atoms, while the opposite was found for the organic cation **Q**, the carborate anion **4** and dianion **5**. This is well in line with the experimentally observed reactivity trend.

The higher affinity of **Q**, **4** and **5** towards electron-rich C=C double bonds in comparison to ions **B**, **1**, **2** and **3** is only tentatively reflected in the calculated reaction enthalpies with **MA** and **ST**. Table 1 lists calculated 0 K reaction enthalpies ΔH_{0K}. Binding to **ST** is in all cases more thermochemically favorable than binding to **MA**. For the radicals with higher nucleophilicity, **1**–**3** and **B**, ΔH_{0K} differences were found to be between 2–5% and for the radicals with higher electrophilicity, **Q**, **4** and **5**, they were between 8–18%. However, electrophilicity and nucleophilicity are reaction kinetic concepts and not necessarily correlated with reaction enthalpy. Instead, barriers along the reaction coordinate are the most concrete descriptors of electrophilic/nucleophilic reactivity. Fast reactions of a radical ion with a neutral reagent in the gas phase proceed *via* transition states that are lower in energy than the separated reagents (formally representing a negative activation energy). However, the measured reaction rates/efficiencies in the gas phase of radical ion-molecule reactions are often lower than the collision rate. This is explained by the TS constituting an entropic bottleneck for the reaction.[83] Differences in TS energies for radical ion–molecule reactions have been correlated with experimentally observed differences in reaction rates, *e.g.*, for addition reactions of unsaturated hydrocarbons like ethylene.[84] Fig. 4 presents an excerpt of the potential energy surface (PES) including TS energy values for the two competing reaction pathways—addition to either **ST** or **MA** —by examining

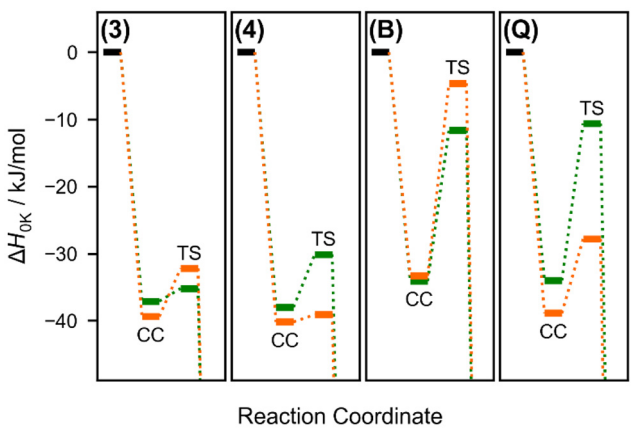

Fig. 4 PES diagrams showing the 0 K reaction enthalpy for the formation of CC, TS and CA between ions **3**, **4**, **B**, and **Q** and **MA** (green paths) or **ST** (orange paths), calculated on M06-2X-D3/def2TZVPP level. Note that the CA states are not explicitly shown. CC = collisional complex, TS = transition state, CA = covalent adduct.

the singly charged electrophilic organic radical ion **Q** and the nucleophilic organic radical ion **B**, as well as the electrophilic borate anion **4** and the nucleophilic borate anion **3**. Energies were computed using the M06-2X hybrid functional that was successfully applied previously for accurate PES modeling of radical ion-molecule reactions.[84] The TS for MA binding (TS (**MA**)) was found energetically below the transition state for ST binding (TS(**ST**)) in the case of **3** and **B**, while the situation is reversed for **4** and **Q**, underlining their conceptual assignment as nucleophilic and electrophilic, respectively.

The described reactions with **MA** and **ST** as well as the cDFT investigations allow us to assign a strong electrophilic character to the radicals **4** and **5** despite their overall negative charge. The electric field near the reactive site of ion **4** supports the attraction of nucleophiles. In the case of ion **5**, however, the electric field does not support a low barrier for the reactions with nucleophiles. The observed reactivity may therefore be the result of a strong thermochemical driving force as can be explained by the high bond dissociation energy (BDE) of O–H.[85]

3.5. Reactions with carbon tetrachloride

To confirm the conceptual categorization as electrophilic and (more) nucleophilic radicals, using a different type of reagent, reactions with carbon tetrachloride (CCl_4) were probed. Halogen atom abstraction (XAT) from electrophilic CCl_4 is associated with nucleophilic radical reactivity[86,87] as deduced from the concept of polarity matching.[88] Fig. 5 demonstrates that the organic electrophilic radical cation **Q** and the borate anion **4** do not react with CCl_4. In contrast, the more nucleophilic radical anion **B** and the borate anion **3** show Cl atom abstraction under the same reaction conditions, further underlining the conceptual categorization (**Q** and **4** electrophilic, **B** and **3** nucleophilic).

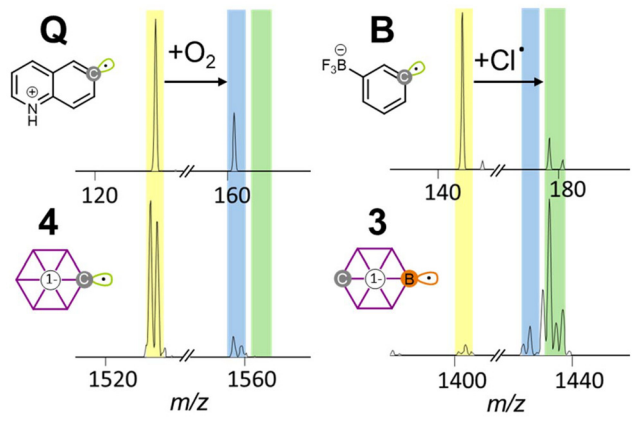

Fig. 5 Mass spectra obtained after 1000 ms reaction between isolated ions **Q**, **B**, **4** and **3** with carbon tetrachloride in the ion trap of a linear quadrupole ion trap mass spectrometer. The ion trap also contained ubiquitous residual O_2 gas. The signal of the isolated radical ion is marked yellow. Ions **B** and **3** react with carbon tetrachloride to form the $Cl^{\bullet}$ abstraction product ions (marked in green). Binding with residual O_2 gas is marked in blue. The mass spectra obtained after 1000 ms reaction time between isolated ions **1** and **2** with CCl_4 are shown in Fig. S9.

3.6. Reactions with allyl iodide

Allyl iodide has been used in a variety of studies over the past decades as a neutral reagent to study radical reactivity of gaseous ions. Distonic phenyl or quinolyl radical cations were shown to primarily abstract I atoms ($I^{\bullet}$) from this reagent.[89,90] Allyl radical ($C_3H_5^{\bullet}$) abstraction and H atom abstraction were either not observed or only observed as minor competing pathway.[37,89,91] Employing the avoided curve-crossing model,[82,92] it has been rationalized that polarization effects are responsible for the experimentally observed preference for I atom abstraction due to a lower-lying transition state.[89] To the best of our knowledge, the competition between allyl radical and I atom abstraction has not been systematically discussed in previous studies. The reported comparisons of distonic radical cations indicate that the allyl radical/I atom abstraction ratio increases as the distonic radical becomes more electrophilic due to additional electron-withdrawing functional groups or reduced spatial separation of the cationic charge-tag.[35,36] However, with increasing electrophilicity, the reaction rate also increases, and the higher allyl radical/I atom abstraction ratio may be the result of an overall lower selectivity, which often accompanies higher reactivity.

Previous studies on the reactions of allyl iodide with anionic radicals are sparse. *meta*-Benzyne diradicals with a negatively charged substituent have been reported not to react with allyl iodide, while a *meta*-benzyne diradical with a positively charged substituent does.[37] The overall electron-rich/nucleophilic character of allyl iodide was proposed to bias its reactions with the anionic diradical. Reactions of allyl iodide with a negatively charged distonic phenyl radical has been reported to occur slowly *via* I atom abstraction.[93] Similarly, in this study, allyl iodide was found to react with anion **B** (see Fig. 6) although slower than cation **Q** (see Fig. S10). However, a minor allyl radical abstraction was also observed in both cases. All anionic borane radicals **1–5** also reacted with allyl iodide, as shown in Fig. 6. In contrast to the organic radicals, I atom abstraction was not observed as the dominant reaction channel. Allyl radical abstraction is the major reaction for ions **1–3**. The I atom abstraction product is substantially more abundant for ion **4** than in case of the other borane anions. In the case of ion **5**, H-atom abstraction dominates (this was also observed for the reactions with **MA** and **ST**; see section 3.3).

Table 2 shows the calculated reaction enthalpies for the three competing pathways (allyl radical abstraction, I atom abstraction and H atom abstraction) for all the ions, **1–5**, **Q** and **B**. A comparison with Fig. 6 shows that the detection of the dominant H atom abstraction only for **5**, and its absence for the other ions, can be explained by thermochemical arguments. In contrast, the competition between allyl radical and I atom abstraction is not simply predictable by the reaction enthalpies. The enthalpies listed in Table 2 do not reflect the experimentally observed tendency of **4**, **Q** and **B** for preferred I atom abstraction, which clearly indicates that the reaction is kinetically controlled and a lower barrier for I atom abstraction than for allyl radical abstraction must control the observed

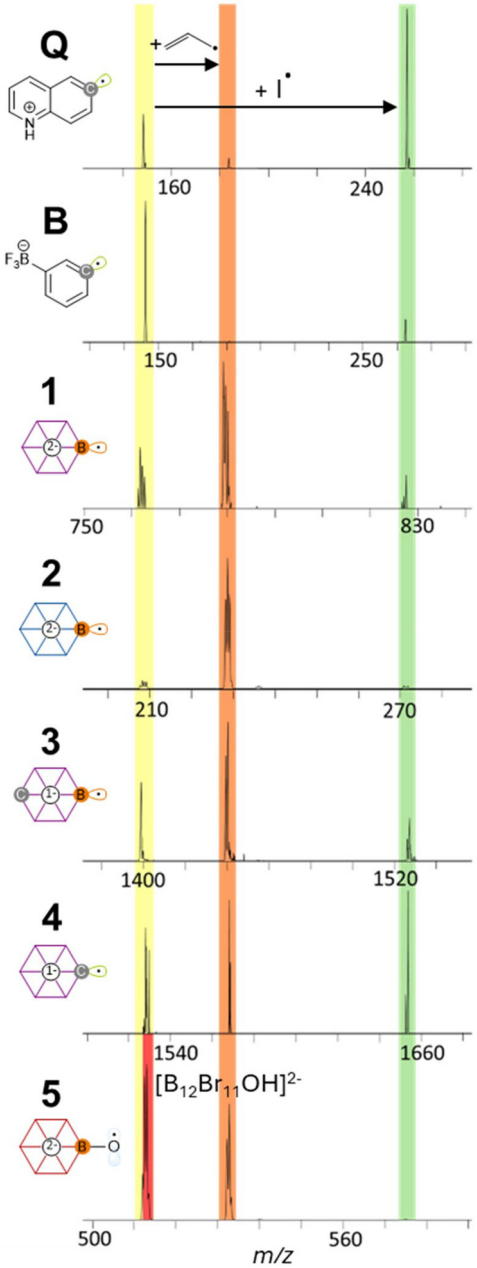

Fig. 6 Mass spectra obtained after 500 ms reaction of isolated ions **Q**, **B**, **1**, **2**, **3**, **4** and **5** with allyl iodide in the ion trap of a linear quadrupole ion trap mass spectrometer. The isolated radical ion is marked in yellow. The allyl radical abstraction and I atom abstraction product ions are marked in orange and green, respectively. In the case of ion **5**, H atom abstraction occurs as the major reaction pathway (marked in red); for details, see Fig. S11.

reactivity in these cases. The experiments shown in Fig. 6 were repeated using allyl chloride instead of allyl iodide (see Fig. S12). Allyl radical abstraction was exclusively observed for all radicals, confirming that the interactions of the radical site with the electron-rich, polarizable iodine atom in allyl iodide is responsible for the kinetic effect. However, the conceptual assignment of all probed ions to nucleophilic or electrophilic

Table 2 0 K reaction enthalpies ΔH_{0K} (B3LYP-D3(BJ)/def2-TZVPP) in kJ mol^{-1} for the competing reaction channels I atom abstraction, allyl radical abstraction and H atom abstraction from allyl iodide by the investigated ions **1**–**5**, **Q** and **B**

Ion	I$^{\bullet}$ atom abstraction	$C_3H_5^{\bullet}$ abstraction	H atom (H$^{\bullet}$) abstraction
Q	−110	−181	−126
B	−122	−149	−102
1	−179	−156	−33
2	−181	−170	−97
3	−174	−157	−82
4	−84	−139	−107
5	3	−86	−92

reactivity (see sections 3.2–3.4) cannot fully explain the different ratios of allyl radical and I atom abstraction: **Q** and **B**, the two organic ions of opposite polarity and opposing electrophilic/nucleophilic character, both show dominant I atom abstraction. Although it was concluded that ion **4** has a similar electrophilicity to **Q**, the allyl radical abstraction product and the I atom abstraction product are similarly abundant for **4**. Apparently, conceptual electrophilic and nucleophilic character of the radical are not the only parameters which determine the transition states for the competing reactions. The similarity of product ratios in the case of **B** and **Q** and the observation that **4** takes an intermediate position by forming both allyl radical and I atom abstraction products in similar abundance leads to the conclusion that parameters like the molecular framework (borane scaffold *vs.* organic aromatic residue) and the element on which the spin density is localized (B *vs.* C) could play a crucial role for the reaction with allyl iodide.

Fig. 7a shows the calculated PES, including separated reagents and TS for the reactions of **1**, **3**, **4**, **B** and **Q** with allyl iodide. The energetics for the attack of the radical *via* the C=C double bond (DB, resulting in allyl radical abstraction) are shown in red. The energetics for attack of the radical *via* iodine (resulting in I atom abstraction) are shown in purple. For **1** and **3**, the PES are qualitatively similar, which is in agreement with the observed reactivity. The energetic barrier for I atom abstraction (TS(I)) is substantial, while only a small and lower-energy barrier (TS(DB)) exists for allyl radical abstraction. This is in line with the experimentally observed preference of allyl radical abstraction for the borane anions **1**–**3** with a vacant boron atom. The energetic difference between the TSs for the abstraction of the iodine atom and the allyl radical is greater for the doubly charged ion **1** than for the singly charged ion **3**. This is in agreement with the experimentally observed slightly higher affinity of ion **1** for allyl radical abstraction as compared to I atom abstraction, than in the case of ion **3** (see Fig. 5 and Fig. S10). In the case of ion **4**, TS (I) is much lower than for **1** and **3**, making this reaction pathway more competitive with the allyl radical abstraction. In contrast, the energetic situation for the anion-tagged phenyl radical **B** appears to be reversed: unlike for the ions **1**, **3** and **4**, as described above, the transition state for attack *via* the double bond (TS(DB)) lies above TS(I). Although this energetic

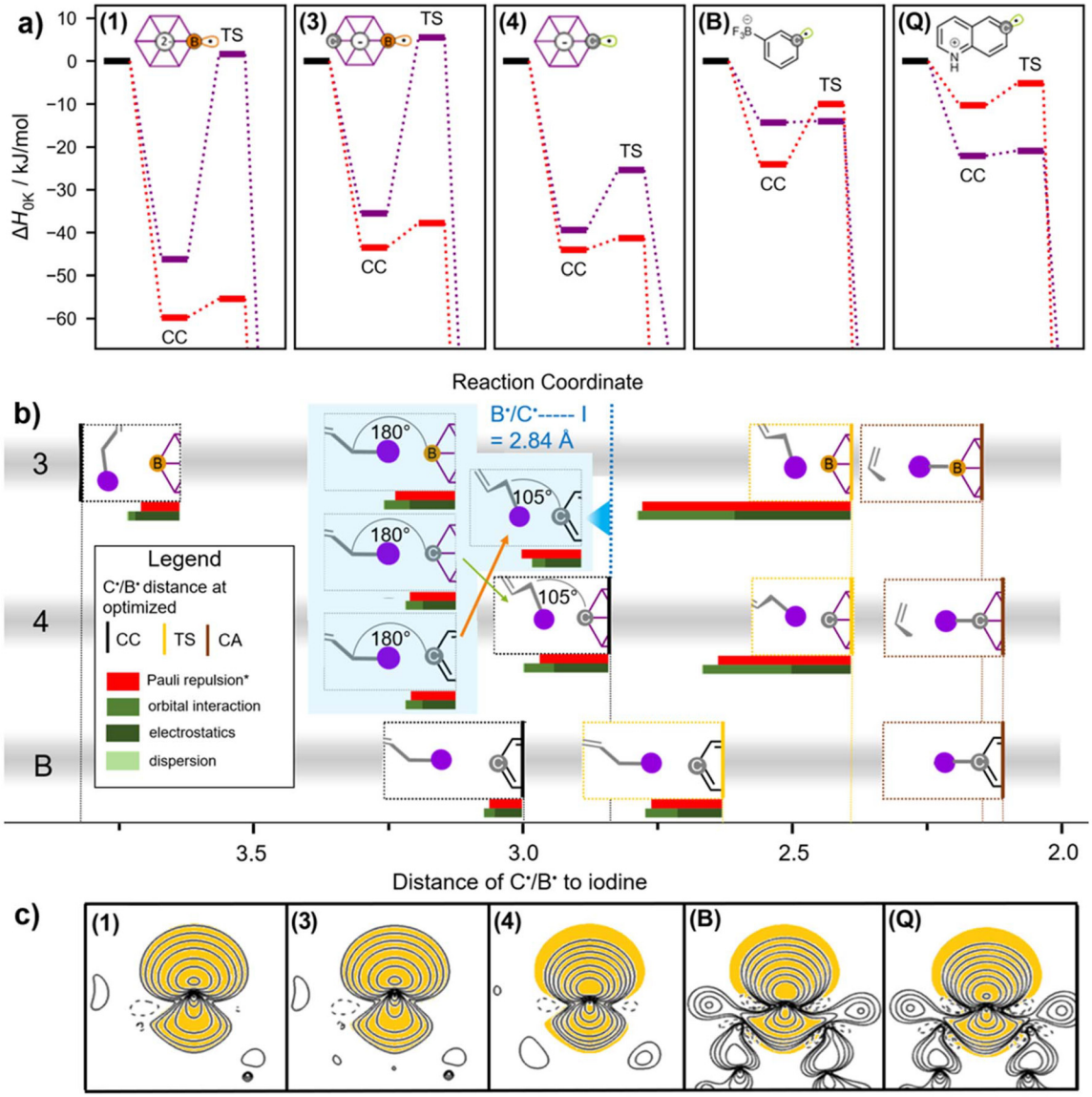

Fig. 7 (a) PES diagrams (M06-2X-D3/def2-TZVPP) for binding of ions **1**, **3**, **4**, **B**, and **Q** to allyl iodide *via* its I atom (purple paths) and the C=C double bond (red paths). Note, that the covalently bound adducts (CA) are not explicitly shown. (b) Excerpts of the optimized geometries of the collision complex (CC) of the reactants (left), TSs (middle), and CAs (right) for binding of ions **3**, **4**, and **B** to allyl iodide, plotted against the distance of the I atom of allyl iodide to the spin-carrying C/B atoms of the ions. (c) Two-dimensional contour line plots of the spin density surrounding ions **1**, **3**, **4**, **B**, and **Q**. Yellow colored areas have equal dimensions in all plots and demonstrate that the spin density in **4**, **B** and **Q** are more compact than in **1** and **3**. *Pauli repulsion refers to the sum $\Delta E_{Pauli} = \Delta E_{xrep} + \Delta E_{DFTc}$ (see section 2.2).

difference between TS(DB) and TS(I) appears small, the reaction for I atom abstraction is almost barrierless, whereas allyl radical abstraction involves a higher-energy TS. The PES for cationic **Q** appears qualitatively similar to that of **B** but TS(I) is even lower in energy, favoring I atom abstraction even stronger than **B**. This is in agreement with the experimental findings (Fig. 5 and Fig. S10). Therefore, all experimentally observed trends for the reactions with allyl iodide as well as **MA** and **ST** are in good agreement with the computed PES. We conclude that DFT models using the M06-2X hybrid functional are well suited for qualitative comparisons and for predicting trends in the reactivity of the studied borane and aryl radical ions.

In order to gain a deeper understanding of the role of the charge on the reactions of borane and phenyl/quinolyl radicals with allyl iodide, the PES for two neutral radicals, $[(HC)_2B_{10}I_9]^\bullet$ and $[C_6H_5]^\bullet$, which cannot be investigated by mass spectrometry, were computed. $[(HC)_2B_{10}I_9]^\bullet$ has the CH groups on the opposite side of the vacant boron atom and hence complements **1** and **3** in a series of borane radicals that only differ by the substitution of B–I with C–H groups. The phenyl radical complements **Q** and **B** in a series of organic radicals with the spin density localized on a carbon atom. A comparison of the PESs can be found in Fig. S13. The PESs support the conclusion that, regardless of the charge state, a high-energy TS(I)

occurs in reactions of the borane radicals, whereas I atom abstraction is almost barrierless and TS(I) is consistently lower in energy than TS(DB) for phenyl/quinolyl radicals. For the latter, TS(DB) lies much higher in energy. Nevertheless, the PESs are modulated by the charge state, in that TS(DB) is energetically stabilized in a series of radicals with increasing negative/lower positive charge. This results in an increasing preference for allyl radical abstraction with more negative/less positive charge on the ions as observed experimentally for both organic and borane radicals.

One possible explanation for the high barrier for I atom abstraction in the case of the borane radical anions could lie in the five sterically demanding iodine substituents that surround the vacant boron atom, while the phenyl/quinolyl radicals appear to be more accessible to allyl iodide. To validate this hypothesis, we computed the PES for the reaction of allyl iodide with the hypothetical derivative $[HCB_{11}F_{10}]^{\bullet-}$ (relating to iodo species **3**) that possesses much smaller F substituents close to the vacant boron site. However, this substitution with fluorine atoms had hardly any effect on the PES (see S14). This is also consistent with the experimentally observed reaction behavior of ions **1** and **2** being almost identical (Fig. 6; I *vs.* CN substituents). Therefore, we conclude that steric or electronic effects of the borane substituents do not influence the barrier height substantially. Carborate anion **4**, with a borane scaffold just like ions **1** and **3** but a carbon atom as the center of spin density (like ions **Q** and **B**), holds an intermediate position in terms of reactivity and barrier height (compare Fig. 6 and 7a). This leads to the hypothesis that the transition states TS(I) and TS(DB), which determine the competition for iodine atom and allyl abstraction, are determined by two different components (i) and (ii):

(i) An element-dependent component of the spin-carrying atom, *i.e.*, a repulsive interaction between the vacant boron atom and the iodine atom in allyl iodide, which is significantly reduced in the case of a vacant carbon atom. This repulsive component plays an important role for the barrier height in **1–3**, but hardly any for ions **4**, **Q** and **B**.

(ii) A framework-dependent interaction, which is similar for borane anions **1–3** and **4**, and in particular, lowers the transition state energy for allyl abstraction compared to the transition state energies observed for phenyl ions.

The strong influence of both, the spin carrying atom and the non-covalent interactions between allyl iodide and the borane/phenyl–moiety becomes evident when analyzing the geometries and interaction energy components of the CC, and the TS for ions **3**, **4** and **B**. Fig. 7b shows this analysis for I atom abstraction. The corresponding geometries for ions **1** and **Q** can be found in S15. For **B**, the C$^{\bullet}$–I–C angle stays 180° during the approach of allyl iodide. In the case of borane anion **3** with a vacant boron atom, the B$^{\bullet}$–I–C angle is 70.4° in the reactant complex, preventing a direct alignment of the I atom of allyl iodide with the vacant boron center. Ion **4** with its C-centered radical represents an intermediate situation with a C$^{\bullet}$–I–C angle of 104.5° for the reactant complex.

Energy decomposition analysis (EDA) within the sobEDA scheme was employed[70] to partition the total interaction energy between the radicals and allyl iodide into the chemically meaningful components: electrostatic interactions, orbital interactions, Pauli repulsion and dispersion interactions. The interaction of allyl iodide in different angles and distances with **3**, **4** and **B** was compared, and the results are shown using a bar chart representation in Fig. 7b. The repulsive Pauli repulsion is shown in red and the attractive components are represented by green bars. This provides a deeper insight into the interactions that cause the different PES for the different types of radicals. First, the interaction of allyl iodide with the three ions was compared by choosing a B$^{\bullet}$/C$^{\bullet}$–I distance of 2.84 Å and a B$^{\bullet}$/C$^{\bullet}$–I–C angle of 180° (see the blue background inset in Fig. 7b). Note that this angle was found only to be favorable for ion **B**. A comparison of the four energy components for ions **B** and **4** shows almost identical values. Apparently, the interactions of the iodine atom of allyl iodide with the carbon-centered radical is similar in both cases and independent of the framework (borane or phenyl). In contrast, in the case of ion **3**, significantly higher values of the energy components are calculated, demonstrating that the substitution of carbon by boron under identical geometrical constraints results in a significantly larger interaction with the iodine atom of allyl iodide. A two-dimensional representation of the spin density in the interaction plane of the radicals with allyl iodide in Fig. 7c shows that the spin density, which is localized at the vacant boron atoms in ions **1** and **3**, is more spatially extended than that localized at the vacant carbon atoms in ions **4**, **B** and **Q**. This is shown by comparison with a yellow-colored surface area, which is equal in all spin density representations. The difference between *C*- and *B*-centered radicals may stem from the "element-specific" difference in electronegativity, which is higher for carbon therefore causing the unpaired electron to get closer to the nucleus (*i.e.*, smaller extension of spin center).

A comparison of the EDA results of the TS(I) structures of ions **3** and **4**, which have the same B$^{\bullet}$/C$^{\bullet}$–I distances of 2.39 Å, show that the larger barrier height for **3** can be rationalized by a 1.5-fold stronger Pauli repulsion. This strong additional repulsion can only be partially compensated by more favorable electrostatic interactions and orbital interactions. Therefore, we conclude that a spatially demanding boron-centered radical contributes to the barrier height observed for ions **1–3** and explains component (i). Based on the aforementioned result that ions **4** and **B** show almost identical interactions with allyl iodide for the 180° B$^{\bullet}$/C$^{\bullet}$–I–C arrangement at 2.84 Å, EDA was used to investigate why reducing the angle is favorable for **4** but not for **B** (compare optimized structures in Fig. 7b; reducing the angle is marked by arrows). Both **B** and **4** show an increase in Pauli repulsion upon decreasing the angle. While this increase in repulsive interactions is not compensated for by attractive components for **B**, a strong increase in attractive electrostatic interactions and orbital interactions occurs for ion **4**. Therefore, different potential energy surfaces for borane and phenyl scaffolds can be attributed to being influenced by

the non-covalent interactions of allyl iodide with the ions. The combination of preferred non-covalent interactions with the borane framework and the less-repulsive interaction with a spin-carrying carbon instead of boron results in the energetically lowest TS(I) for **4** in the series of investigated ions. For the competing allyl abstraction, the spin carrying atom was found to play no important role for the energy of the transition state. EDA of TS(DB) structures shows that in particular electrostatic interactions are responsible for a stronger stabilization of TS(DB) in borane ions like **3** and **4** as compared to, e.g., **B** (see Table S2), explaining component (ii).

The described influences on the reaction barriers for the reactions of the borane radical ions **1–5** and organic radical ions **Q** and **B** with allyl iodide are determined by several aspects, which at first glance are not directly related to the intuitive concept of nucleophilicity and electrophilicity of radicals. However, it should be noted that the two highly electrophilic ions **4** and **Q** exhibit the energetically lowest-lying TS(I)s (Fig. 7a), which contributes to the enhanced I atom abstraction affinities in the respective series of borane and organic radical ions. However, the competition between allyl radical and I atom abstraction for the probed ions can only be fully understood by considering the Pauli repulsion of *B- vs. C*-localized radicals and the interactions of allyl iodide with the ionic framework of the radical.

4. Conclusion

The chemical character of the five *closo*-borate anion derivatives $[B_{12}I_{11}]^{\bullet 2-}$ (**1**), $[B_{12}(CN)_{11}]^{\bullet 2-}$ (**2**), $[HCB_{11}I_{10}]^{\bullet -}$ (**3**), $[B_{11}I_{11}C]^{\bullet -}$ (**4**) and $[B_{12}Br_{11}O]^{\bullet 2-}$ (**5**) with localized spin density has been explored and characterized by comparison with a quinoline radical cation **Q** and a BF_3-substituted phenyl radical anion **B**. The reactivity of the oxygen-localized radical **5** is mainly determined by the strong thermochemical driving force for H atom abstraction. Therefore, despite its dianionic charge, a similar reactivity was observed as known for phenoxy radicals. The reactivity of the other radicals with a boron or carbon atom-localized radical site is governed by kinetic effects. Comparison of the competing binding of the double bonds of electron-deficient methyl acrylate and electron-richer styrene leads to the conclusion that dianions **1** and **2** are nucleophilic radicals but still show some binding with styrene, which was not observed for anion **B**. This nucleophilic character is reduced for anion **3**. For anion **4** (despite its negative charge), a strong electrophilic character has to be assigned, also evidenced by binding properties similar to cation **Q**.

However, using electrophilicity and nucleophilicity to categorize the observed binding preferences reaches its limitation when the reaction with allyl iodide is considered. The borane radical anions with the spin density localized on boron atoms (**1–3**) show preferred allyl radical abstraction, while the phenyl ions **Q** and **B** (independent of their polarity) show preferred iodine atom abstraction. Ion **4** constitutes an intermediate position. These observations were explained as follows: (i) the spatial extension of the spin density is greater in the case of a boron-centered radical than in the case of carbon-centered radical, resulting in more repulsive interactions with the electron cloud of the iodine atom (*i.e.*, greater Pauli repulsion) for **1–3** than for the C-centered radicals **4**, **Q** and **B**. (ii) Interactions of the allyl residue with the three-dimensional *closo*-borane framework result in a different geometry of CC and TS for **1–4** than for **Q** and **B** with their two-dimensional aromatic framework. An energetically low-lying TS for DB binding in the case of borate radical anions as compared to the phenyl-based radicals can be traced back to a substantial increase in the electrostatic interactions for the borate radical anions. This demonstrates how both element-specific properties of the spin-carrying atom and interactions of the bulky borane scaffold with molecular groups of the reaction partner are important for understanding the details of the reactivity of *closo*-borate radical anions.

Comparing the experimentally obtained results with the computational descriptors demonstrates the ability of these methods to accurately predict the chemical reactivity of *closo*-borate anion radicals. Notably, using the M06-2X functional to reliably model CCs and corresponding TSs reproduces experimental trends for competing reactions—specifically, **MA** *vs.* **ST** binding and iodine atom *vs.* allyl radical abstraction from allyl iodide. It should be noted that the B3LYP functional failed to reliably locate CC structures on the PES (local minima prior to TS) in our investigations. Analyzing electric fields in front of the reactive radical site does successfully predict the trends observed for ions **1–4**. In particular, the electrophilic reactivity of carborane **4** is rationalized by reduced repulsion of negative point charges approaching the radical site of the anion. However, it should be noted that the electric field alone does not predict the electrophilic properties of dianion **5** that are not based on the partial charge on the spin-carrying atom. Conceptual DFT investigations qualitatively align with experimentally observed trends in nucleophilicity and electrophilicity, however, it was found that "artificial neutralization" of the investigated system is required, which has not been used in previous investigations using conceptual DFT for ionic radicals. We propose that including a counterion spatially separated from the radical site should become a standard for conceptual DFT investigations of ions. The necessity for such a neutralization in the computational investigation becomes obvious by the exceptional case of ion **4** (a strongly electrophilic, anionic radical), which is otherwise predicted to be strongly nucleophilic by conceptual DFT.

The conceptualization of ionic radicals presented here may form a basis to understand the chemical nature of uncommon ionic radicals that are formed as intermediates in (photochemical) reactions. Furthermore, these radicals may be applied for direct bond forming preparative chemistry after generation and mass selection in the gas phase and their soft-landing into layers of reagents on surfaces using preparative mass spectrometry.

Conflicts of interest

The authors declare no conflict of interest.

Data availability

Data for this article, including input and output files of computational investigations and raw data files of mass spectrometry investigations are available at ioChem-BD at **https://doi.org/10.19061/iochem-bd-6-587** and at PURR Publications at **https://purr.purdue.edu/publications/4966/1**.

Supplementary information (SI) is available. See DOI: **https://doi.org/10.1039/d5qi02163d**.

Acknowledgements

J. W. is grateful to the Volkswagen foundation for a Freigeist Fellowship and the Exploration Grants program of the Boehringer Ingelheim Foundation (BIS). Funding by the Deutsche Forschungsgemeinschaft (DFG, German Research Foundation) Project 498397108 and TRR 325 – 444632635 (for K. Z.) is gratefully acknowledged. Computations for this work were done with resources of Leipzig University Computing Center. J. K. is grateful to Purdue University for the Bilsland Dissertation Fellowship.

References

1 J. J. Garwood, A. D. Chen and D. A. Nagib, Radical Polarity, *J. Am. Chem. Soc.*, 2024, **146**(41), 28034–28059, DOI: **10.1021/jacs.4c06774**.

2 F. De Vleeschouwer, V. Van Speybroeck, M. Waroquier, P. Geerlings and F. De Proft, Electrophilicity and Nucleophilicity Index for Radicals, *Org. Lett.*, 2007, **9**(14), 2721–2724, DOI: **10.1021/ol071038k**.

3 P. Geerlings, F. De Proft and W. Langenaeker, Conceptual Density Functional Theory, *Chem. Rev.*, 2003, **103**(5), 1793–1874, DOI: **10.1021/cr990029p**.

4 M. Maiuri, M. Garavelli and G. Cerullo, Ultrafast Spectroscopy: State of the Art and Open Challenges, *J. Am. Chem. Soc.*, 2020, **142**(1), 3–15, DOI: **10.1021/jacs.9b10533**.

5 Y. Gauduel, S. Pommeret, A. Migus, N. Yamada and A. Antonetti, Femtosecond Investigation of Single-Electron Transfer and Radical Reactions in Aqueous Media and Bioaggregate-Mimetic Systems, *J. Opt. Soc. Am. B*, 1990, **7**(8), 1528–1539, DOI: **10.1364/JOSAB.7.001528**.

6 J.-C. Gumy and E. Vauthey, Investigation of the Excited-State Dynamics of Radical Ions in the Condensed Phase Using the Picosecond Transient Grating Technique, *J. Phys. Chem. A*, 1997, **101**(46), 8575–8580, DOI: **10.1021/jp972066v**.

7 R. Ismail and J. H. Tannous, Free Radical Quantification in Chemical Systems: Challenges and Future Perspectives, *Chem. Eng. Res. Des.*, 2024, **210**, 97–111, DOI: **10.1016/j.cherd.2024.08.021**.

8 K. M. Stirk, L. K. M. Kiminkinen and H. I. Kenttamaa, Ion-Molecule Reactions of Distonic Radical Cations, *Chem. Rev.*, 1992, **92**(7), 1649–1665, DOI: **10.1021/cr00015a008**.

9 A. Dreuw and L. S. Cederbaum, Multiply Charged Anions in the Gas Phase, *Chem. Rev.*, 2002, **102**(1), 181–200, DOI: **10.1021/cr0104227**.

10 X.-B. Wang and L.-S. Wang, Photoelectron Spectroscopy of Multiply Charged Anions, *Annu. Rev. Phys. Chem.*, 2009, **60**(1), 105–126, DOI: **10.1146/annurev.physchem.59.032607.093724**.

11 P. E. Williams, D. L. Marshall, B. L. J. Poad, V. R. Narreddula, B. B. Kirk, A. J. Trevitt and S. J. Blanksby, Comparing Positively and Negatively Charged Distonic Radical Ions in Phenylperoxyl Forming Reactions, *J. Am. Soc. Mass Spectrom.*, 2018, **29**(9), 1848–1860, DOI: **10.1007/s13361-018-1988-9**.

12 J. Warneke and X.-B. Wang, Measuring Electronic Structure of Multiply Charged Anions to Understand Their Chemistry: A Case Study on Gaseous Polyhedral *closo*-Borate Dianions, *J. Phys. Chem. A*, 2021, **125**(31), 6653–6661, DOI: **10.1021/acs.jpca.1c04618**.

13 L. Wang, Y. Jiang, S. Duttwyler, F. Lin and Y. Zhang, Chemistry of Three-Dimensional Icosahedral Boron Clusters Anions: *closo*-Dodecaborate (2-) $[B_{12}H_{12}]^{2-}$ and Carba-*closo*-Dodecaborate(-) $[CB_{11}H_{12}]^{-}$, *Coord. Chem. Rev.*, 2024, **516**, 215974, DOI: **10.1016/j.ccr.2024.215974**.

14 I. B. Sivaev, V. I. Bregadze and N. T. Kuznetsov, Derivatives of the *closo*-Dodecaborate Anion and Their Application in Medicine, *Russ. Chem. Bull.*, 2002, **51**(8), 1362–1374, DOI: **10.1002/chin.200311239**.

15 L. Wang, W. Sun, Y. Zhang, N. Xu, R. Krishna, J. Hu, Y. Jiang, Y. He and H. Xing, Interpenetration Symmetry Control within Ultramicroporous Robust Boron Cluster Hybrid MOFs for Benchmark Purification of Acetylene from Carbon Dioxide, *Angew. Chem., Int. Ed.*, 2021, **60**(42), 22865–22870, DOI: **10.1002/anie.202107963**.

16 Y. Zhang, J. Hu, R. Krishna, L. Wang, L. Yang, X. Cui, S. Duttwyler and H. Xing, Rational Design of Microporous MOFs with Anionic Boron Cluster Functionality and Cooperative Dihydrogen Binding Sites for Highly Selective Capture of Acetylene, *Angew. Chem., Int. Ed.*, 2020, **59**(40), 17664–17669, DOI: **10.1002/anie.202007681**.

17 Y. Zhang, L. Yang, L. Wang, S. Duttwyler and H. Xing, A Microporous Metal–organic Framework Supramolecularly Assembled from a CuII Dodecaborate Cluster Complex for Selective Gas Separation, *Angew. Chem., Int. Ed.*, 2019, **58**(24), 8145–8150, DOI: **10.1002/anie.201903600**.

18 W. Sun, Y. Jin, Y. Wu, W. Lou, Y. Yuan, S. Duttwyler, L. Wang and Y. Zhang, A New Boron Cluster Anion Pillared Metal Organic Framework with Ligand Inclusion and Its Selective Acetylene Capture Properties, *Inorg. Chem. Front.*, 2022, **9**(20), 5140–5147, DOI: **10.1039/D2QI00890D**.

19 I. B. Sivaev, V. I. Bregadze and S. Sjöberg, Chemistry of *closo*-Dodecaborate Anion $[B_{12}H_{12}]^{2-}$: A Review, *Collect. Czech. Chem. Commun.*, 2002, **67**(6), 679–727, DOI: **10.1135/cccc20020679**.

20 X. Zhao, Z. Yang, H. Chen, Z. Wang, X. Zhou and H. Zhang, Progress in Three-Dimensional Aromatic-like *closo*-Dodecaborate, *Coord. Chem. Rev.*, 2021, **444**, 214042, DOI: 10.1016/j.ccr.2021.214042.

21 J. C. Axtell, L. M. Saleh, E. A. Qian, A. I. Wixtrom and A. M. Spokoyny, Synthesis and Applications of Perfunctionalized Boron Clusters, *Inorg. Chem.*, 2018, **57**(59), 2333–2350, DOI: 10.1021/acs.inorgchem.7b02912.

22 J. Warneke, G.-L. Hou, E. Aprà, C. Jenne, Z. Yang, Z. Qin, K. Kowalski, X.-B. Wang and S. S. Xantheas, Electronic Structure and Stability of $[B_{12}X_{12}]^{2-}$ (X = F–At): A Combined Photoelectron Spectroscopic and Theoretical Study, *J. Am. Chem. Soc.*, 2017, **139**(41), 14749–14756, DOI: 10.1021/jacs.7b08598.

23 M. Mayer, V. van Lessen, M. Rohdenburg, G.-L. Hou, Z. Yang, R. M. Exner, E. Aprà, V. A. Azov, S. Grabowsky, S. S. Xantheas, K. R. Asmis, X.-B. Wang, C. Jenne and J. Warneke, Rational Design of an Argon-Binding Superelectrophilic Anion, *Proc. Natl. Acad. Sci. U. S. A.*, 2019, **116**(17), 8167–8172, DOI: 10.1073/pnas.1820812116.

24 C. Knapp, Weakly Coordinating Anions: Halogenated Borates and Dodecaborates, in *Comprehensive Inorganic Chemistry II*, ed. J. Reedijk and K. Poeppelmeier, Elsevier, 2013, vol. 1, pp. 651–679, DOI: 10.1016/978-0-08-097774-4.00125-X.

25 M. Mayer, M. Rohdenburg, V. Van Lessen, M. C. Nierstenhöfer, E. Aprà, S. Grabowsky, K. R. Asmis, C. Jenne and J. Warneke, First Steps towards a Stable Neon Compound: Observation and Bonding Analysis of $[B_{12}(CN)_{11}Ne]^-$, *Chem. Commun.*, 2020, **56**(33), 4591–4594, DOI: 10.1039/D0CC01423K.

26 M. Rohdenburg, M. Mayer, M. Grellmann, C. Jenne, T. Borrmann, F. Kleemiss, V. A. Azov, K. R. Asmis, S. Grabowsky and J. Warneke, Superelectrophilic Behavior of an Anion Demonstrated by the Spontaneous Binding of Noble Gases to $[B_{12}Cl_{11}]^-$, *Angew. Chem., Int. Ed.*, 2017, **56**(27), 7980–7985, DOI: 10.1002/anie.201702237.

27 X. Ma, M. Rohdenburg, H. Knorke, S. Kawa, J. K.-Y. Liu, E. Aprà, K. R. Asmis, V. A. Azov, J. Laskin, C. Jenne, H. I. Kenttämaa and J. Warneke, Binding of Saturated and Unsaturated C_6 -Hydrocarbons to the Electrophilic Anion $[B_{12}Br_{11}]^-$: A Systematic Mechanistic Study, *Phys. Chem. Chem. Phys.*, 2022, **24**(36), 21759–21772, DOI: 10.1039/D2CP01042A.

28 J. Warneke, M. Mayer, M. Rohdenburg, X. Ma, J. K. Y. Liu, M. Grellmann, S. Debnath, V. A. Azov, E. Apra, R. P. Young, C. Jenne, G. E. Johnson, H. I. Kenttämaa, K. R. Asmis and J. Laskin, Direct Functionalization of C–H Bonds by Electrophilic Anions, *Proc. Natl. Acad. Sci. U. S. A.*, 2020, **117**(38), 23374–23379, DOI: 10.1073/pnas.2004432117.

29 R. T. Boeré, J. Derendorf, C. Jenne, S. Kacprzak, M. Keßler, R. Riebau, S. Riedel, T. L. Roemmele, M. Rühle, H. Scherer, T. Vent-Schmidt, J. Warneke and S. Weber, On the Oxidation of the Three–Dimensional Aromatics $[B_{12}X_{12}]^{2-}$ (X=F, Cl, Br, I), *Chem. – Eur. J.*, 2014, **20**(15), 4447–4459, DOI: 10.1002/chem.201304405.

30 J. Warneke, M. Rohdenburg, J. K. Y. Liu, E. Johnson, X. Ma, R. Kumar, P. Su, E. Aprà, X.-B. Wang, C. Jenne, M. Finze, H. I. Kenttämaa and J. Laskin, Gas Phase Fragmentation of Adducts between Dioxygen and *closo*-Borate Radical Anions, *Int. J. Mass Spectrom.*, 2019, **436**, 71–78, DOI: 10.1016/j.ijms.2018.11.005.

31 M. E. Kilic and P. Jena, Catalytic Potential of $[B_{12}X_{11}]^{2-}$ (X = F, Cl, Br, I, CN), Dianions, *J. Phys. Chem. Lett.*, 2023, **14**(39), 8697–8701, DOI: 10.1021/acs.jpclett.3c02222.

32 B. Giese, Formation of CC Bonds by Addition of Free Radicals to Alkenes, *Angew. Chem., Int. Ed. Engl.*, 1983, **22**(10), 753–764, DOI: 10.1002/anie.198307531.

33 A. M. Spokoyny, C. D. Lewis, G. Teverovskiy and S. L. Buchwald, Extremely Electron-Rich, Boron-Functionalized, Icosahedral Carborane-Based Phosphinoboranes, *Organometallics*, 2012, **31**(24), 8478–8481, DOI: 10.1021/om301116x.

34 R. B. King, Three-Dimensional Aromaticity in Polyhedral Boranes and Related Molecules, *Chem. Rev.*, 2001, **101**(5), 1119–1152, DOI: 10.1021/cr000442t.

35 X. Ma, R. O. Anyaeche, E. Feng, E. Johnson, E. Roller, D. J. Rumley, J. J. Nash and H. I. Kenttämaa, Gas-Phase Reactivity of Quinoline-Based Singlet Oxenium Cations, *J. Org. Chem.*, 2024, **89**(8), 5458–5468, DOI: 10.1021/acs.joc.3c02895.

36 R. R. Kotha, R. Yerabolu, M. S. Aqueel, J. S. Riedeman, L. Szalwinski, D. Ding, J. J. Nash and H. I. Kenttämaa, Quinoline Triradicals: A Reactivity Study, *J. Am. Chem. Soc.*, 2019, **141**(16), 6672–6679, DOI: 10.1021/jacs.9b01740.

37 J. M. Price, K. E. Nizzi, J. L. Campbell, H. I. Kenttämaa, M. Seierstad and C. J. Cramer, Experimental and Theoretical Characterization of the 3,5-Didehydrobenzoate Anion: A Negatively Charged *meta* -Benzyne, *J. Am. Chem. Soc.*, 2003, **125**(1), 131–140, DOI: 10.1021/ja021112o.

38 R. G. Parr, L. V. Szentpály and S. Liu, Electrophilicity Index, *J. Am. Chem. Soc.*, 1999, **121**(9), 1922–1924, DOI: 10.1021/ja983494x.

39 H. A. Mills, J. L. Martin, A. L. Rheingold and A. M. Spokoyny, Oxidative Generation of Boron-Centered Radicals in Carboranes, *J. Am. Chem. Soc.*, 2020, **142**(10), 4586–4591, DOI: 10.1021/jacs.0c00300.

40 H. Ren, P. Zhang, J. Xu, W. Ma, D. Tu, C. Lu and H. Yan, Direct B–H Functionalization of Icosahedral Carboranes *via* Hydrogen Atom Transfer, *J. Am. Chem. Soc.*, 2023, **145**(13), 7638–7647, DOI: 10.1021/jacs.3c01314.

41 S. Li and Z. Xie, Visible-Light-Promoted Nickel-Catalyzed Cross-Coupling of Iodocarboranes with (Hetero)Arenes via Boron-Centered Carboranyl Radicals, *J. Am. Chem. Soc.*, 2022, **144**(18), 7960–7965, DOI: 10.1021/jacs.2c02329.

42 M. Chen, J. Xu, D. Zhao, F. Sun, S. Tian, D. Tu, C. Lu and H. Yan, Site–Selective Functionalization of Carboranes at the Electron–Rich Boron Vertex: Photocatalytic B–C Coupling via a Carboranyl Cage Radical, *Angew. Chem., Int. Ed.*, 2022, **61**(37), e202205672, DOI: 10.1002/anie.202205672.

43 C. Selg, W. Neumann, P. Lönnecke, E. Hey-Hawkins and K. Zeitler, Carboranes as Aryl Mimetics in Catalysis: A

Highly Active Zwitterionic NHC–Precatalyst, *Chem. – Eur. J.*, 2017, **23**(33), 7932–7937, DOI: 10.1002/chem.201700209.

44 M. Saleh, D. R. Powell and R. J. Wehmschulte, Chlorination of 1-Carba-*closo* -Dodecaborate and 1-Ammonio- *Closo* -Dodecaborate Anions, *Inorg. Chem.*, 2016, **55**(20), 10617–10627, DOI: 10.1021/acs.inorgchem.6b01867.

45 S. Xu, H. Zhang, J. Zong, H. Cao, D. Tu, C. Lu and H. Yan, Taming Inert B–H Bond with Low Energy Light: A Near-Infrared Light-Induced Approach to Facile Carborane Cluster-Amino Acid Coupling, *J. Am. Chem. Soc.*, 2025, **147**(15), 12845–12857, DOI: 10.1021/jacs.5c01610.

46 F. Paulus, C. Heusel, M. Jaspers, L. M. Amrehn, F. Schreiner, D. Rana, C. G. Daniliuc, M. R. Hansen and F. Glorius, *Closo*–Carboranyl Analogs of β–Arylethylamines: Direct Synthesis from Alkenes via EnT–Catalysis, *Angew. Chem., Int. Ed.*, 2025, **64**(27), e202504793, DOI: 10.1002/anie.202504793.

47 A. Lanfranco, P. Renzi, M. Rusconi and A. Deagostino, Carboranes Meet Photochemistry: Recent Progresses in Light-Mediated Cage Functionalisation, *Tetrahedron Lett.*, 2023, **131**, 154782, DOI: 10.1016/j.tetlet.2023.154782.

48 M. Rohdenburg, Z. Warneke, H. Knorke, M. Icker and J. Warneke, Chemical Synthesis with Gaseous Molecular Ions: Harvesting $[B_{12}Br_{11}N_2]^-$ from a Mass Spectrometer, *Angew. Chem., Int. Ed.*, 2023, **62**(45), e202308600, DOI: 10.1002/anie.202308600.

49 S. Kawa, J. Kaur, H. Knorke, Z. Warneke, M. Wadsack, M. Rohdenburg, M. Nierstenhöfer, C. Jenne, H. Kenttämaa and J. Warneke, Generation and Reactivity of the Fragment Ion $[B_{12}I_8S(CN)]^-$ in the Gas Phase and on Surfaces, *Analyst*, 2024, **149**(9), 2573–2585, DOI: 10.1039/d3an02175k.

50 F. Yang, K. A. Behrend, H. Knorke, M. Rohdenburg, A. Charvat, C. Jenne, B. Abel and J. Warneke, Anion–Anion Chemistry with Mass–Selected Molecular Fragments on Surfaces, *Angew. Chem., Int. Ed.*, 2021, **60**(47), 24910–24914, DOI: 10.1002/anie.202109249.

51 S. Gronert, Mass Spectrometric Studies of Organic Ion/Molecule Reactions, *Chem. Rev.*, 2001, **101**(2), 329–360, DOI: 10.1021/cr9900836.

52 M. J. Frisch, G. W. Trucks, H. B. Schlegel, G. E. Scuseria, M. A. Robb, J. R. Cheeseman, G. Scalmani, V. Barone, G. A. Petersson, H. Nakatsuji, X. Li, M. Caricato, A. V. Marenich, J. Bloino, B. G. Janesko, R. Gomperts, B. Mennucci, H. P. Hratchian, J. V. Ortiz, A. F. Izmaylov, J. L. Sonnenberg, D. Williams-Young, F. Ding, F. Lipparini, F. Egidi, J. Goings, B. Peng, A. Petrone, T. Henderson, D. Ranasinghe, V. G. Zakrzewski, J. Gao, N. Rega, G. Zheng, W. Liang, M. Hada, M. Ehara, K. Toyota, R. Fukuda, J. Hasegawa, M. Ishida, T. Nakajima, Y. Honda, O. Kitao, H. Nakai, T. Vreven, K. Throssell, J. A. Jr., J. E. Peralta, F. Ogliaro, M. J. Bearpark, J. J. Heyd, E. N. Brothers, K. N. Kudin, V. N. Staroverov, T. A. Keith, R. Kobayashi, J. Normand, K. Raghavachari, A. P. Rendell, J. C. Burant, S. S. Iyengar, J. Tomasi, M. Cossi, J. M. Millam, M. Klene, C. Adamo, R. Cammi, J. W. Ochterski, R. L. Martin, K. Morokuma, O. Farkas, J. B. Foresman, and D. *J. Fox, Gaussian*, Vol. 16, Revision C. 02, Gaussian. Inc, Wallingford CT, 2019.

53 A. D. Becke, Density-Functional Thermochemistry., III. The Role of Exact Exchange, *J. Chem. Phys.*, 1993, **98**(7), 5648–5652, DOI: 10.1063/1.464913.

54 C. Lee, W. Yang and R. G. Parr, Development of the Colle-Salvetti Correlation-Energy Formula into a Functional of the Electron Density, *Phys. Rev. B:Condens. Matter Mater. Phys.*, 1988, **37**(2), 785–789, DOI: 10.1103/PhysRevB.37.785.

55 B. Miehlich, A. Savin, H. Stoll and H. Preuss, Results Obtained with the Correlation Energy Density Functionals of Becke and Lee, Yang and Parr, *Chem. Phys. Lett.*, 1989, **157**(3), 200–206, DOI: 10.1016/0009-2614(89)87234-3.

56 F. Weigend and R. Ahlrichs, Balanced Basis Sets of Split Valence, Triple Zeta Valence and Quadruple Zeta Valence Quality for H to Rn: Design and Assessment of Accuracy, *Phys. Chem. Chem. Phys.*, 2005, **7**(18), 3297–3305, DOI: 10.1039/B508541A.

57 S. Grimme, J. Antony, S. Ehrlich and H. Krieg, A Consistent and Accurate Ab Initio Parametrization of Density Functional Dispersion Correction (DFT-D) for the 94 Elements H-Pu, *J. Chem. Phys.*, 2010, **132**(15), 154104, DOI: 10.1063/1.3382344.

58 S. Grimme, S. Ehrlich and L. Goerigk, Effect of the Damping Function in Dispersion Corrected Density Functional Theory, *J. Comput. Chem.*, 2011, **32**(7), 1456–1465, DOI: 10.1002/jcc.21759.

59 Y. Zhao and D. G. Truhlar, The M06 Suite of Density Functionals for Main Group Thermochemistry, Thermochemical Kinetics, Noncovalent Interactions, Excited States, and Transition Elements: Two New Functionals and Systematic Testing of Four M06-Class Functionals and 12 Other Functionals, *Theor. Chem. Acc.*, 2008, **120**(1–3), 215–241, DOI: 10.1007/s00214-007-0310-x.

60 O. J. Shiels, P. D. Kelly, C. C. Bright, B. L. J. Poad, S. J. Blanksby, G. Da Silva and A. J. Trevitt, Reactivity Trends in the Gas-Phase Addition of Acetylene to the *N* -Protonated Aryl Radical Cations of Pyridine, Aniline, and Benzonitrile, *J. Am. Soc. Mass Spectrom.*, 2021, **32**(2), 537–547, DOI: 10.1021/jasms.0c00386.

61 P. D. Kelly, C. C. Bright, S. J. Blanksby, G. Da Silva and A. J. Trevitt, Molecular Weight Growth in the Gas-Phase Reactions of Dehydroanilinium Radical Cations with Propene, *J. Phys. Chem. A*, 2019, **123**(41), 8881–8892, DOI: 10.1021/acs.jpca.9b04088.

62 D. Caraiman and D. K. Bohme, Periodic Trends in Reactions of Benzene Clusters of Transition Metal Cations, $M(C_6H_6)_{1,2}^+$, with Molecular Oxygen, *J. Phys. Chem. A*, 2002, **106**(42), 9705–9717, DOI: 10.1021/jp0208900.

63 S. F. Boys and F. Bernardi, The Calculation of Small Molecular Interactions by the Differences of Separate Total Energies. Some Procedures with Reduced Errors, *Mol. Phys.*, 1970, **19**(4), 553–566, DOI: 10.1080/00268977000101561.

64 S. Simon, M. Duran and J. J. Dannenberg, How Does Basis Set Superposition Error Change the Potential Surfaces for

Hydrogen-Bonded Dimers?, *J. Chem. Phys.*, 1996, **105**(24), 11024–11031, DOI: 10.1063/1.472902.

65 T. Lu, A Comprehensive Electron Wavefunction Analysis Toolbox for Chemists, Multiwfn, *J. Chem. Phys.*, 2024, **161**(8), 082503, DOI: 10.1063/5.0216272.

66 T. Lu and F. Chen, Multiwfn: A Multifunctional Wavefunction Analyzer, *J. Comput. Chem.*, 2012, **33**(5), 580–592, DOI: 10.1002/jcc.22885.

67 T. Lu and Q. Chen, Realization of Conceptual Density Functional Theory and Information–Theoretic Approach in Multiwfn Program, in *Conceptual Density Functional Theory*, ed. S. Liu, Wiley, 2022, pp. 631–647. DOI: 10.1002/9783527829941.ch31.

68 F. Neese, Software Update: The ORCA Program System, Version 4.0, *Wiley Interdiscip. Rev.:Comput. Mol. Sci.*, 2018, **8**(1), e1327, DOI: 10.1002/wcms.1327.

69 F. Neese, F. Wennmohs, U. Becker and C. Riplinger, The ORCA Quantum Chemistry Program Package, *J. Chem. Phys.*, 2020, **152**(22), 224108, DOI: 10.1063/5.0004608.

70 T. Lu and Q. Chen, Simple, Efficient, and Universal Energy Decomposition Analysis Method Based on Dispersion-Corrected Density Functional Theory, *J. Phys. Chem. A*, 2023, **127**(33), 7023–7035, DOI: 10.1021/acs.jpca.3c04374.

71 F. M. Bickelhaupt and E. J. Baerends, Kohn–Sham Density Functional Theory: Predicting and Understanding Chemistry, *Rev. Comput. Chem.*, 2000, 1–86, DOI: 10.1002/9780470125922.ch1.

72 T. Ziegler and A. Rauk, On the Calculation of Bonding Energies by the Hartree Fock Slater Method: I. The Transition State Method, *Theor. Chim. Acta*, 1977, **46**, 1–10, DOI: 10.1007/BF02401406.

73 K. Kitaura and K. Morokuma, A New Energy Decomposition Scheme for Molecular Interactions within the Hartree–Fock Approximation, *Int. J. Quantum Chem.*, 1976, **10**(2), 325–340, DOI: 10.1002/qua.560100211.

74 Z. Xie, C.-W. Tsang, E. T.-P. Sze, Q. Yang, D. T. W. Chan and T. C. W. Mak, Highly Chlorinated, Brominated, and Iodinated Icosahedral Carborane Anions: 1-H-$CB_{11}X_{11}^-$, 1-CH_3-$CB_{11}X_{11}^-$ (X = Cl, Br, I); 1-Br-$CB_{11}Br_{11}^-$, *Inorg. Chem.*, 1998, **37**(25), 6444–6451, DOI: 10.1021/ic9805628.

75 V. Geis, K. Guttsche, C. Knapp, H. Scherer and R. Uzun, Synthesis and Characterization of Synthetically Useful Salts of the Weakly-Coordinating Dianion $[B_{12}Cl_{12}]^{2-}$, *Dalton Trans.*, 2009, **15**, 2687, DOI: 10.1039/b821030f.

76 I. Tiritiris and T. Schleid, Die Kristallstrukturen der Dicaesium–Dodekahalogeno–*closo*–Dodekaborate $Cs_2[B_{12}X_{12}]$ (X= Cl, Br, I) und ihrer Hydrate, *Z. Anorg. Allg. Chem.*, 2004, **630**(11), 1555–1563, DOI: 10.1002/zaac.200400167.

77 K. R. Asmis, B. B. Beele, C. Jenne, S. Kawa, H. Knorke, M. C. Nierstenhöfer, X. Wang, J. Warneke, Z. Warneke and Q. Yuan, Synthesis, Electronic Properties and Reactivity of $[B_{12}X_{11}(NO_2)]^{2-}$ (X=F–I) Dianions, *Chem. – Eur. J.*, 2020, **26**(64), 14594–14601, DOI: 10.1002/chem.202003537.

78 A. Himmelspach, J. A. P. Sprenger, J. Warneke, M. Zähres and M. Finze, Mercury(II) Complexes of the Carba- *Closo* -Dodecaboranyl Ligands [*closo*-1-CB_{11} X_{11}]$^{2-}$ (X = H, F, Cl, Br, I), *Organometallics*, 2012, **31**(4), 1566–1577, DOI: 10.1021/om201023h.

79 K. M. Stirk, J. C. Orlowski, D. T. Leeck and H. I. Kenttamaa, The Identification of Distonic Radical Cations on the Basis of a Reaction with Dimethyl Disulfide, *J. Am. Chem. Soc.*, 1992, **114**(22), 8604–8606, DOI: 10.1021/ja00048a038.

80 R. C. Dunbar, Infrared Radiative Cooling of Gas–phase Ions, *Mass Spectrom. Rev.*, 1992, **11**(4), 309–339, DOI: 10.1002/mas.1280110403.

81 M. Mayer, M. Rohdenburg, S. Kawa, F. Horn, H. Knorke, C. Jenne, R. Tonner, K. R. Asmis and J. Warneke, Relevance of π–Backbonding for the Reactivity of Electrophilic Anions $[B_{12}X_{11}]^-$ (X=F, Cl, Br, I, CN), *Chem. – Eur. J.*, 2021, **27**(40), 10274–10281, DOI: 10.1002/chem.202100949.

82 T. Mondal, S. Shaik, H. Kenttämaa and T. Stuyver, Modulating the Radical Reactivity of Phenyl Radicals with the Help of Distonic Charges: It Is All about Electrostatic Catalysis, *Chem. Sci.*, 2021, **12**(13), 4800–4809, DOI: 10.1039/D0SC07111K.

83 M. J. Pellerite and J. I. Brauman, Intrinsic Barriers in Nucleophilic Displacements, *J. Am. Chem. Soc.*, 1980, **102**(19), 5993–5999, DOI: 10.1021/ja00539a003.

84 O. J. Shiels, J. A. Turner, P. D. Kelly, S. J. Blanksby, G. Da Silva and A. J. Trevitt, Modelling Reaction Kinetics of Distonic Radical Ions: A Systematic Investigation of Phenyl-Type Radical Addition to Unsaturated Hydrocarbons, *Faraday Discuss.*, 2022, **238**, 475–490, DOI: 10.1039/D2FD00045H.

85 Y.-R. Luo, *Comprehensive Handbook of Chemical Bond Energies*, CRC Press, 2007, DOI: DOI: 10.1201/9781420007282.

86 B. P. Roberts, Polarity-Reversal Catalysis of Hydrogen-Atom Abstraction Reactions: Concepts and Applications in Organic Chemistry, *Chem. Soc. Rev.*, 1999, **28**(1), 25–35, DOI: 10.1039/a804291h.

87 M. Maldonado-Domínguez and M. Srnec, Quantifiable Polarity Match Effect on C–H Bond Cleavage Reactivity and Its Limits in Reaction Design, *Dalton Trans.*, 2023, **52**(5), 1399–1412, DOI: 10.1039/D2DT04018B.

88 L. Yang, T. Bekele, M. A. Lipton and H. I. Kenttämaa, Generation and Characterization of a Distonic Biradical Anion Formed from an Enediynone Prodrug in the Gas Phase, *J. Am. Soc. Mass Spectrom.*, 2013, **24**(4), 563–572, DOI: 10.1007/s13361-012-0567-8.

89 J. L. Heidbrink, K. K. Thoen and H. I. Kenttämaa, Polar Effects on Iodine Atom Abstraction by Charged Phenyl Radicals, *J. Org. Chem.*, 2000, **65**(3), 645–651, DOI: 10.1021/jo981911i.

90 P. E. Williams, B. J. Jankiewicz, L. Yang and H. I. Kenttämaa, Properties and Reactivity of Gaseous Distonic Radical Ions with Aryl Radical Sites, *Chem. Rev.*, 2013, **113**(9), 6949–6985, DOI: 10.1021/cr400121w.

91 X. Ma, C. Jin, D. Wang, J. J. Nash and H. I. Kenttämaa, Relative Reactivities of Three Isomeric Aromatic Biradicals with a 1,4–Biradical Topology Are Controlled by Polar Effects, *Chem. – Eur. J.*, 2019, **25**(25), 6355–6361, DOI: 10.1002/chem.201806106.

92 N. M. Donahue, J. S. Clarke and J. G. Anderson, Predicting Radical–Molecule Barrier Heights: The Role of the Ionic Surface, *J. Phys. Chem. A*, 1998, **102**(22), 3923–3933, DOI: **10.1021/jp980372i**.

93 C. J. Petzold, E. D. Nelson, H. A. Lardin and H. I. Kenttämaa, Charge-Site Effects on the Radical Reactivity of Distonic Ions, *J. Phys. Chem. A*, 2002, **106**(42), 9767–9775, DOI: **10.1021/jp025521i**.